MOLECULAR ONCOLOGY 9 (2015) 335–354

available at www.sciencedirect.com

ScienceDirect

www.elsevier.com/locate/molonc

SNAIL1 combines competitive displacement of ASCL2 and epigenetic mechanisms to rapidly silence the *EPHB3* tumor suppressor in colorectal cancer

Kerstin Rönsch[a,b], Sabine Jägle[a,b], Katja Rose[a], Maximilian Seidl[c,d], Francis Baumgartner[e], Vivien Freihen[a], Afsheen Yousaf[f], Eric Metzger[g,h,i], Silke Lassmann[c,h,i], Roland Schüle[g,h,i], Robert Zeiser[e,h], Tom Michoel[f,j], Andreas Hecht[a,b,h,*]

[a]Institute of Molecular Medicine and Cell Research, Albert-Ludwigs-University Freiburg, Stefan-Meier-Str. 17, 79104 Freiburg, Germany
[b]Faculty of Biology, Albert-Ludwigs-University Freiburg, Schänzlestr. 1, 79104 Freiburg, Germany
[c]Department of Pathology, University Medical Center, Breisacher Str. 115a, 79106 Freiburg, Germany
[d]Center for Chronic Immunodeficiency, University Medical Center, Breisacher Str. 117, 79106 Freiburg, Germany
[e]Department of Hematology and Oncology, University Medical Center, Hugstetter Str. 55, 79106 Freiburg, Germany
[f]Freiburg Institute for Advanced Studies (FRIAS), Albert-Ludwigs-University Freiburg, Albertstraße 19, 79104 Freiburg, Germany
[g]Department of Urology/Women's Hospital and Center for Clinical Research, University Medical Center, Breisacher Str. 66, 79106 Freiburg, Germany
[h]BIOSS Centre for Biological Signalling Studies, Albert-Ludwigs-University Freiburg, Schänzlestr. 18, 79104 Freiburg, Germany
[i]German Consortium for Translational Cancer Research (DKTK) and German Cancer Research Center (DKFZ), Im Neuenheimer Feld 280, 69120 Heidelberg, Germany
[j]The Roslin Institute, The University of Edinburgh, Easter Bush, Midlothian EH25 9RG, Scotland, UK

ARTICLE INFO

Article history:
Received 5 August 2014
Received in revised form
27 August 2014

ABSTRACT

EPHB3 is a critical cellular guidance factor in the intestinal epithelium and an important tumor suppressor in colorectal cancer (CRC) whose expression is frequently lost at the adenoma-carcinoma transition when tumor cells become invasive. The molecular mechanisms underlying *EPHB3* silencing are incompletely understood. Here we show that *EPHB3* expression is anti-correlated with inducers of epithelial-mesenchymal transition (EMT) in

Abbreviations: ASCL2, Achaete-scute family bHLH transcription factor 2; bHLH, basic helix-loop-helix; CDK, cyclin-dependent kinase; CDX, Caudal type homeobox; ChIP, chromatin immunoprecipitation; CRC, colorectal cancer; Dox, doxycycline; E-Cad, E-Cadherin; EMSA, electrophoretic mobility shift assay; EMT, epithelial-mesenchymal transition; EPHB2, EPH receptor B2; EPHB3, EPH receptor B3; ETS, v-ets avian erythroblastosis virus E26 oncogene homolog; FAIRE, Formaldehyde-Assisted Isolation of Regulatory Elements; FFPE, formalin-fixed and paraffin-embedded; HA, hemagglutinin; HDAC, histone deacetylase; HE, hematoxylin and eosin; ISC, intestinal stem cell; LDA, limiting dilution assay; LEF1, Lymphoid enhancer factor 1; LGR5, Leucine-rich repeat containing G protein-coupled receptor 5; LSD1, lysine (K)-specific demethylase 1A; MAPK, mitogen-activated protein kinase; OLFM4, Olfactomedin 4; PC, principal component; PRC2, Polycomb repressive complex 2; qRT-PCR, quantitative reverse transcriptase PCR; RLA, relative luciferase activity; SEM, standard error of the mean; SNAG, Snail/Gfi1; SOPs, standard operating procedures; TBE, TCF/LEF binding element; TCF, T-cell factor; TCGA, The Cancer Genome Atlas; TCP, tranylcypromine; ZEB1, Zinc finger E-box binding homeobox 1.

* *Corresponding author.* Institute of Molecular Medicine and Cell Research, Albert-Ludwigs-University Freiburg, Stefan-Meier-Str. 17, D-79104 Freiburg, Germany. Tel.: +49 761 203 9608; fax: +49 761 203 9602.
E-mail address: andreas.hecht@mol-med.uni-freiburg.de (A. Hecht).

http://dx.doi.org/10.1016/j.molonc.2014.08.016

Accepted 29 August 2014
Available online 16 September 2014

Keywords:
Colorectal cancer
Epithelial-mesenchymal transition
Epigenetic regulation
Snail1
EPHB3

primary tumors and CRC cells. *In vitro*, SNAIL1 and SNAIL2, but not ZEB1, repress *EPHB3* reporter constructs and compete with the stem cell factor ASCL2 for binding to an E-box motif. At the endogenous *EPHB3* locus, SNAIL1 triggers the displacement of ASCL2, p300 and the Wnt pathway effector TCF7L2 and engages corepressor complexes containing HDACs and the histone demethylase LSD1 to collapse active chromatin structure, resulting in rapid downregulation of *EPHB3*. Beyond its impact on *EPHB3*, SNAIL1 deregulates markers of intestinal identity and stemness and *in vitro* forces CRC cells to undergo EMT with altered morphology, increased motility and invasiveness. In xenotransplants, SNAIL1 expression abrogated tumor cell palisading and led to focal loss of tumor encapsulation and the appearance of areas with tumor cells displaying a migratory phenotype. These changes were accompanied by loss of *EPHB3* and *CDH1* expression. Intriguingly, SNAIL1-induced phenotypic changes of CRC cells are significantly impaired by sustained EPHB3 expression both *in vitro* and *in vivo*. Altogether, our results identify *EPHB3* as a novel target of SNAIL1 and suggest that disabling EPHB3 signaling is an important aspect to eliminate a roadblock at the onset of EMT processes.

1. Introduction

Colorectal cancer (CRC) is one of the most frequent forms of cancer worldwide (American Cancer Society, 2013). As with other tumor entities, CRC-related mortality increases sharply with the occurrence of metastasis whereby tumor cells become invasive and disseminate to ultimately colonize secondary tissues (Valastyan and Weinberg, 2011). In colorectal tumorigenesis, signaling by EPHB receptor tyrosine kinases represents a powerful barrier against tumor cell spreading (Batlle et al., 2005; Chiu et al., 2009). *EPHB3* is one of the EPHB family members that is expressed in the healthy intestinal epithelium and acts as a cellular guidance and positioning factor with crucial functions in the maintenance of intestinal crypt architecture (Batlle et al., 2002; Holmberg et al., 2006). The histoarchitectural function of EPHB3 likely explains its invasion and tumor suppressor capacity in CRC. Repulsive interactions between cells expressing the EPHB3 receptor and EphrinB ligands, respectively, compartmentalize tumors and thereby impede detachment of cells from the primary tumor (Batlle et al., 2005; Cortina et al., 2007). Moreover, EPHB/EphrinB signaling affects intracellular distribution and function of the cell–cell adhesion molecule E-Cadherin and thus contributes to the stabilization of a non-invasive epithelial cell phenotype (Chiu et al., 2009; Cortina et al., 2007; Solanas et al., 2011).

EMT is a process that facilitates tumor cell invasion and dissemination in many different cancers (Kalluri and Weinberg, 2009). In the course of EMT, epithelial cell characteristics such as the expression of E-Cadherin and apical-basal polarity are lost and replaced by mesenchymal traits including increased motility and invasiveness. EMT can be induced in different ways, most notably by a group of transcriptional repressor proteins including SNAIL1, SNAIL2 and ZEB1 which recognize specific DNA-binding sites within regulatory regions of their target genes, so called E-boxes (Peinado et al., 2007). E-boxes are also bound by many basic helix-loop-helix (bHLH) developmental regulators leading to competition among these factors and EMT-inducing repressors (Soleimani et al., 2012). Additionally, EMT inducers can recruit multicomponent corepressor complexes to inactivate their target genes. For example, the N-terminal SNAG domain of SNAIL1 and SNAIL2 interacts with protein complexes containing histone deacetylases (HDACs), the histone demethylase LSD1/KDM1A and the Polycomb repressive complex 2 (PRC2) (Lin et al., 2010a, 2010b; Peinado et al., 2004; von Burstin et al., 2009). HDACs and LSD1 collectively remove activating histone marks from target gene loci while PRC2 deposits the repressive histone modification H3K27me3 to shut down gene expression.

In the intestinal epithelium, *EPHB3* is expressed in multiple cell-types including intestinal stem cells (ISCs), transit amplifying cells and Paneth cells located in the lower part of intestinal crypts (Batlle et al., 2002; Itzkovitz et al., 2012). The maintenance and generation of these cell populations requires the coordinated activity of Wnt/β-catenin, Notch and mitogen-activated protein kinase (MAPK) signaling and several transcription factors including the bHLH protein ASCL2 (van der Flier and Clevers, 2009). These signaling cascades and transcription factors are also critically involved in the regulation of *EPHB3* both in the healthy intestinal epithelium and in tumorigenesis. *EPHB3* is a direct target gene of Wnt/β-catenin and Notch signaling (Batlle et al., 2002; Jägle et al., 2014; Rodilla et al., 2009) and in agreement with the pivotal role of these pathways in tumor initiation (Fre et al., 2009; van Es et al., 2005), *EPHB3* is strongly upregulated in colorectal adenomas (Batlle et al., 2005; Chiu et al., 2009; Rönsch et al., 2011). However, this surge in *EPHB3* expression at early stages of tumorigenesis is followed by secondary downregulation in up to 30% of carcinomas. Intriguingly, we recently identified a transcriptional enhancer located 2.3 kb upstream of the *EPHB3* promoter (Jägle et al., 2014) which collects and computes input from Wnt/β-catenin, Notch and MAPK signaling, ETS transcription factors and ASCL2 to drive *EPHB3* expression. Even more importantly, decommissioning of the *EPHB3* enhancer appears to play a central role in *EPHB3* secondary silencing. In this regard we previously identified a defect in Notch signaling that contributes to *EPHB3* enhancer inactivation but defective Notch signaling cannot completely

explain *EPHB3* enhancer incapacitation and *EPHB3* silencing (Jägle et al., 2014). Of note, recent studies showed that colorectal cancer is a rather heterogeneous disease that can be categorized into several molecularly distinct subtypes that differ in their genetic and epigenetic make-up and the ensuing disturbances in tumor-relevant signaling pathways (Cancer Genome Atlas, 2012; De Sousa et al., 2013; Loboda et al., 2011; Marisa et al., 2013; Sadanandam et al., 2013). In view of the apparent CRC heterogeneity it is conceivable that also the deregulation of *EPHB3* can be multifaceted and involves different mechanisms.

The increasingly recognized impact of EMT in CRC (Hwang et al., 2014, 2011; Loboda et al., 2011; Shioiri et al., 2006; Wang et al., 2010) prompted us to investigate a potential role of EMT-inducing transcriptional repressors in *EPHB3* enhancer decommissioning and *EPHB3* secondary silencing. Here, we report that the expression of *EPHB3* and EMT inducers is inversely correlated in tumors and CRC cell lines, and we identify *EPHB3* as a novel and direct target of SNAIL1/SNAIL2. Mechanistically, SNAIL1/SNAIL2 appear to competitively displace the ISC factor ASCL2 from a common E-box binding motif and to engage HDACs and LSD1 to disable the *EPHB3* enhancer thereby downregulating *EPHB3* expression. Interestingly, sustained expression of EPHB3 can partially suppress SNAIL1-induced EMT features *in vitro* and *in vivo* suggesting that incapacitation of EPHB3 signaling is a critical step to promote EMT processes in colorectal cancer.

2. Materials and methods

2.1. Plasmid construction

To generate luciferase reporter constructs covering *EPHB3* upstream regions, a plasmid with sequences up to position −1624 bp in pGL3basic (a gift of T. Brabletz, Freiburg, Germany) was used as a starting construct. Further luciferase reporter plasmids where derived from this construct by polymerase chain reaction (PCR) amplification of *EPHB3* sequences from genomic DNA of LS174T cells and standard cloning techniques. The *EPHB3* E-box was mutated according to the Stratagene QuikChange site-directed mutagenesis protocol using the following primer: 5′-GGATGTGTTGCTGCCAGGAACCGTCCT GAAATATCTCTGTGTCC-3′ (mutated bases are underlined). Constructs were sequence verified. The expression vectors pCS2+Snail1; pcDNA3-Snail1-HA, pRetro-X-tight-Pur-SNAIL1 were kindly provided by M. Stemmler (Freiburg, Germany), A. García de Herreros (Barcelona, Spain) and H. Munshi (Chicago, IL, USA), respectively. The ASCL2 coding region was amplified by PCR using cDNA from LS174T cells as template with the following primer pair: 5′-GGATCCGCGATG GACGGCGGCACACT-3′;

5′-TTCGAAGTAGCCCCCTAACCAGCTGGA-3′. The resulting PCR product was cut with BamHI and BstBI and ligated into pCS2+ carrying the coding region for a hemagglutinin (HA)-tag. To generate pCS2+SNAIL2-HA, the coding region for SNAIL2 was cut out from pcDNA3-SNAIL2 (a gift of T. Brabletz, Freiburg, Germany) with KpnI and EcoRI and ligated into pCS2+ carrying the coding region for an HA-tag. pCS2+ZEB1 was generated by cutting out the coding region for ZEB1 from pCI-neo-ZEB1 (a gift of T. Brabletz, Freiburg, Germany) with XbaI and XhoI and ligating it into the pCS2+ vector. To generate pCS2+Snail1-HA-ΔSNAG, Snail1 was amplified by PCR using the following primer pair: 5′-GGATCCATGTCC GACCCCCGCCGGAAGCCC-3′; 5′-GAATTCGCGAGGGCCTCCG GAGCAGCC-3′ which allowed cutting out the PCR product lacking the SNAG domain with BamHI and EcoRI and ligating it into pCS2+ carrying the coding region for an HA-tag. For the generation of stable, Dox-inducible cell lines, the coding regions for Snail1-HA and Snail1-HA-ΔSNAG were transferred into the pRetroX-tight-Pur vector (Clontech, Saint-Germain-en-Laye, France) by standard cloning techniques. To construct DLD1 cells stably expressing HA-tagged Snail1, the pRetroX-tight-Pur vector was modified to additionally carry the reverse tetracycline controlled transactivator rtTA3 under the control of the UbqC promoter isolated from the pTRIPZ vector (Open Biosystems/Thermo Fisher Scientific, Dreieich, Germany). To generate the lentiviral expression vector for EPHB3, the puromycin resistance gene in FUW-CMV-EPHB3-IRES-puro (a gift of E. Batlle, Barcelona, Spain), was replaced with the blasticidin resistance. For the corresponding control vector, the coding region of EPHB3 was cut out using BamHI and AgeI. Details about cloning strategies are available upon request.

2.2. Cell culture

The CRC cell lines LS174T (CLS #300392) and HT29 (CLS #300215) were obtained from the Cell Line Service culture collection (DKFZ, Heidelberg) and ATCC, respectively. SW480, HCT116 and HEK293 cell lines were obtained from the Max-Planck-Institute of Immunobiology, Freiburg. The LS411 cell line was provided by Tilman Brummer (Freiburg, Germany). The Caco2 cell line was provided by Oliver Schilling (Freiburg, Germany). The CRC cell line DLD1 and the pancreatic carcinoma cell lines Panc1 and Capan2 were provided by Thomas Brabletz (Freiburg, Germany). The human breast carcinoma cell lines MDA-MB231 and MCF7 were provided by Thomas Reinheckel (Freiburg, Germany), and the oesophageal squamous cell carcinoma cell lines OE21 and OE23 were provided by Silke Lassmann (Freiburg, Germany). Cells were cultured as previously described (Rönsch et al., 2011). Stable cell lines were generated by retroviral infection with pRetroX-tight-Pur-based vectors as described (Wallmen et al., 2012) except for the generation of stable cell lines constitutively expressing EPHB3 which were made with lentiviral vectors. As recipients, HT29 and LS174T cells stably transfected with the pN1pβactin-rtTA2S-M2-IRES-EGFP plasmid (Welman et al., 2006) were used. To inhibit LSD1 and HDACs, cells were treated for 24 h with 10 μM tranylcypromine (TCP) or 3 μM MS275, respectively.

2.3. Migration analyses and spheroid formation

Migration was either analyzed by scratch assay (Liang et al., 2007) or in real-time using the xCELLigence™ system (Roche, Mannheim, Germany). For the scratch assay, 1×10^6 cells per well were seeded in 6-well plates. 6 h later, when cells were firmly attached, the cell monolayer was wounded in a straight line using a 200 μl pipette tip. Cell debris was carefully removed by washing the cells with PBS. Fresh medium

containing 0.1 μg/ml Dox was added to the cells. Phase contrast pictures were taken with the Axiovert microscope (Zeiss, Oberkochen, Germany). To monitor migration continuously, the xCELLigence™ system was used according to the supplier's instruction manual. Briefly, a two-chamber setup (CIM-Plate-16™) with microelectronic sensors on the underside of the upper chamber was employed and 8×10^4 cells, pre-treated for 72 h with 0.1 μg/ml Dox, were seeded in serum-free DMEM in the upper chamber. DMEM containing 10% FCS was added to the lower chamber to attract cells. Real-time monitoring of cell migration was performed for 12 h in 30 min intervals.

2.4. Spheroid formation

Spheroid formation was allowed in a collagen I matrix. Cells were harvested and suspended in cell culture medium supplemented with of 0.24% (w/v) methylcellulose and 0.1 μg/ml Dox to form droplets containing approximately 500 cells. Droplets were applied to cell culture plates which were subsequently turned upside down and incubated for 24 h at 37 °C to allow spheroid formation. The next day, spheroids were collected by carefully washing them from the plates using PBS. For embedding the spheroids in a collagen I matrix containing 0.6% methylcellulose, 24-well plates were used which had previously been coated with collagen I. One hour after embedding the spheroids, medium containing 0.1 μg/ml Dox was added. 48 h later, phase contrast pictures of the spheroids were taken as described above and the length of invasive sprouts as well as the number of sprouts per spheroid were measured using the Axiovision LE 4.4 software (Zeiss, Oberkochen, Germany).

2.5. Limiting dilution assay (LDA)

LDA was used to asses sphere forming capacity as an indicator of self-renewal properties of LS174T CRC cell derivatives (O'Brien et al., 2012). Defined cell numbers ranging from 10,000 to 0.0001 cells per well were seeded and cultivated in 96-well ultra-low attachment plates in stem cell media (DMEM/F12 advanced, 1 x B27 supplement, 20 ng/ml EGF and 10 ng/ml FGF). For each cell number 8 replicates were prepared. Cells were either left untreated or were treated with 0.1 μg/ml Dox which was refreshed every 48 h. Sphere formation was analyzed 7 days later by counting the number of wells in which spheres were detectable. These data were processed using the ELDA software (http://bioinf.wehi.edu.au/software/elda/) (Hu and Smyth, 2009). Phase contrast pictures were taken with the Axiovert microscope (Zeiss, Oberkochen, Germany). For sphere formation in the second generation, spheres from the eight wells in which originally 10,000 cells had been seeded, were pooled, cells were dissociated, counted and cell numbers ranging from 1000 to 0.001 were seeded. Dox treatment was performed as described. Again, sphere formation was analyzed 7 days later.

2.6. Analysis of population dynamics by crystal violet staining

For the analysis of cell culture dynamics, 0.5×10^5 cells were seeded in duplicates in 24 well plates. 6 h after seeding, cells were either harvested (time point 0 h) or treated with 0.1 μg/ml Dox for 24, 48, 72 or 96 h. After 48 h, Dox was renewed. For staining, cells were washed with PBS before 0.5% crystal violet in 20% methanol was added. After incubation for 10 min with gentle agitation cells were washed four times with ddH_2O. Subsequently, crystal violet was extracted with 100% methanol for 30 min and duplicate absorbance measurements at 595 nm were performed with 1:100 dilutions of the extracted dye (Hirsch et al., 2007).

2.7. Luciferase reporter assays

For luciferase reporter assays, 1×10^5 LS174T cells were seeded in 24-well plates and transfected using FuGENE6 reagent (Promega, Mannheim, Germany) according to the manufacturer's protocol. For luciferase assays testing activities of the *EPHB3* and *CDH1* reporter constructs, the cells received a mixture of 10 ng of the Renilla luciferase expression vector pRL-CMV for internal standardization, 250 ng of firefly luciferase reporters driven by *EPHB3* DNA fragments or driven by the *CDH1* DNA fragment, respectively, and 100 ng of plasmid DNA for expression of Snail1-HA, Snail1-HA-ΔSNAG, SNAIL2-HA, ZEB1 or CtBP1. To analyze the competition between ASCL2-HA and Snail1-HA at the *EPHB3* luciferase reporter constructs, 50 ng of pCS2+ASCL2-HA and increasing amounts of pCS2+Snail1 (either 50 ng, 100 ng or 200 ng) were transfected. In order to analyze Wnt/β-catenin pathway activity, 10 ng of the Renilla luciferase expression vector pRL-CMV and 500 ng of the firefly luciferase reporter plasmids pSuper8xTOPFlash or pSuper8xFOPFlash were transfected (Veeman et al., 2003). To keep the total amount of transfected DNA constant, appropriate amounts of the empty expression vectors were added. Cell lysates were prepared and reporter activity was determined as described (Wallmen et al., 2012) 45–48 h after transfection. Renilla luciferase activity was used for normalization.

2.8. RNA interference

For knockdown studies, cells were seeded in 6-well plates (1×10^6 cells/well) and transfected with 20 nM of siRNAs directed against HDAC1, HDAC2, HDAC3, HDAC7 and HDAC8 (M-003493-02-0005, M-003495-02-005, M-003496-02-005, M-009330-02-0005 and M-003500-02-0005, respectively, Dharmacon, Lafayette, USA) using Lipofectamine® 2000 (Invitrogen/Life Technologies, Darmstadt, Germany). 16 h after transfection, cells were washed once with PBS and RNA was isolated 72 h post transfection.

2.9. RNA isolation, cDNA synthesis and RT-PCR

Total RNA was isolated using the peqGOLD total RNA kit (PeqLab, Erlangen, Germany). Complementary DNA (cDNA) synthesis and reverse transcriptase (RT)-PCR were performed as previously described (Wallmen et al., 2012). For RT-PCR an equivalent of 50 ng total RNA was used as template. Quantitative RT-PCR (qRT-PCR) was performed with the iQ5 or CFX-96 multicolor real-time PCR detection systems (BioRad, Munich, Germany) using SYBR green reaction mix (PeqLab, Erlangen, Germany). A cDNA amount equivalent to 20 ng total RNA was used as template. Data were normalized to *GAPDH*

expression. Values shown represent expression of the genes-of-interest relative to *GAPDH* unless stated otherwise. Primers are listed in the Supplementary Table S1.

2.10. Western blotting and immunodetection

For immunodetection experiments whole cell lysates were prepared. For this, cells were lysed in IPN-150 [50 mM Tris/HCl pH 7.6, 150 mM NaCl, 5 mM $MgCl_2$, 0.1% NP40, Complete™ protease inhibitor (Roche Applied Science, Mannheim, Germany), 1 mM DTT, 0.1 mM Na_3VO_4, 1 mM PMSF and 10 mM NaF] for 30 min on ice. Cell lysates were cleared by centrifugation at 18,500 × *g* and 4 °C for 10 min. Protein concentrations were determined using the DC protein detection kit (BioRad, Munich, Germany). Proteins were separated by SDS-polyacrylamide gel electrophoresis (SDS-PAGE) and transferred on nitrocellulose membranes. The antibodies used for immunodetection are listed in Supplementary Table S2. Visualization of antibody:antigen complexes was performed as described (Weise et al., 2010).

2.11. Co-immunoprecipitation

Protein–protein interactions were analyzed by co-immunoprecipitation using whole cell lysates. For the comparative analyses of interactions between Snail1-HA, Snail1-ΔSNAG-HA and corepressors, HEK293 cells were transfected with expression vectors for Snail1-HA and Snail1-ΔSNAG-HA. For this, 1×10^7 cells were seeded in 15 cm dishes. 4 h later they were transfected with 1.5 ml of a calcium phosphate-DNA co-precipitate using 10 μg of the appropriate DNA. 45–48 h after transfection, cells were lysed in IPN-150. 750 μg of the protein lysate were subjected to immunoprecipitation at 4 °C overnight with 1 μg anti-HA-antibody (3F10; Roche Applied Science, Mannheim, Germany), or goat immunoglobulin G (sc-2028; Santa Cruz, Heidelberg, Germany) and magnetic protein G dynabeads (Life Technologies, Darmstadt, Germany). Precipitates were washed three times with IPN-150 buffer before resuspending the beads in 2× protein loading buffer and boiling for 5 min. Proteins were analyzed by Western blotting.

2.12. Electrophoretic mobility shift assay (EMSA)

DNA binding *in vitro* was analyzed by EMSA as described (Weise et al., 2010). For this, proteins used were transcribed and translated *in vitro* using the TNT SP6 high-yield wheat germ protein expression system with 2.5 μg of the respective plasmid DNA in 25 μl reactions according to the manufacturer's protocol (Promega, Heidelberg, Germany). Protein expression was confirmed by Western blot. DNA probes for EMSA were generated by PCR with biotinylated primers using *EPHB3* upstream sequences as DNA template. 10 fMol of the biotinylated probe were combined with equal amounts of the specific protein, the reaction was supplemented with 60 μg of bovine serum albumin and 1 μg of poly(dI:dC) and incubated in EMSA-buffer [20 mM Hepes pH7.9, 75 mM NaCl, 2 mM $MgCl_2$, Complete™ protease inhibitor (Roche Applied Science, Mannheim, Germany), 1 mM DTT] for 30 min on ice. Subsequently, reactions were loaded onto 6% polyacrylamide gels with 0.5 × Tris-borate-EDTA running buffer and further processed using the Chemiluminescent nucleic acid detection module (Thermo Fisher Scientific, Dreieich, Germany).

2.13. Formalydehyde-assisted isolation of regulatory elements (FAIRE)

FAIRE was performed as described (Giresi et al., 2007). The cells used for the experiments were either left untreated to serve as reference material or were crosslinked with 1% formaldehyde for 7 min. Sonification was performed with 300 μl aliquots of each sample for 20 cycles with 30 s on/30 s off at high amplitude settings in a Bioruptor Plus (Diagenode, Liège, Belgium), yielding DNA fragments between 250 and 750 bp in length. qPCR was conducted using 40 ng of DNA recovered from crosslinked cells and non-crosslinked reference material. Data calculation was done as described (Wallmen et al., 2012). Primer sequences are listed in Supplementary Table S1.

2.14. Chromatin immunoprecipitation (ChIP)

ChIP analyses were carried out as described (Wallmen et al., 2012) with 100 μg or 200 μg of 1% formaldehyde-crosslinked chromatin. All antibodies used are listed in Supplementary Table S2. qPCR was performed using 1 μl of precipitated DNA and 2% input material as template with primers listed in Supplementary Table S1. Data were calculated as %-input or as %-input relative to H3 to compensate for variations in nucleosome density.

2.15. Pairwise correlation and principal component analyses of microarray gene expression data

The pairwise Pearson correlation coefficient between 23 genes of interest was calculated from normalized RNA-Seq gene expression levels in 270 samples of stage I to IV colon and rectum carcinomas obtained from The Cancer Genome Atlas (TCGA) (Cancer Genome Atlas, 2012). Data tables were downloaded from https://tcga-data.nci.nih.gov/docs/publications/coadread_2012/. In the pairwise correlation matrix, genes were clustered using single linkage with Euclidean distance. To estimate the correlation between the EMT inducer cluster (cluster 1: *SNAI2*, *VIM*, *ZEB2*, *FN1*, *ZEB1*, *TWIST1*, *TWIST2*, *SNAI2*; see Figure 1A) and the EPHB3 cluster (cluster 2: *EPHB2*, *EPHB3*, *EPHB4*, *CDX1*, *CDX2*, *ASCL2*, *AXIN2*, *CDH1*; see Figure 1A), we calculated the Pearson correlation between the first principal component or "eigengene" of each cluster (Alter et al., 2000; Langfelder and Horvath, 2007). Briefly, the TCGA expression data was log-transformed and standardised such that each gene had mean expression level zero and unit standard deviation over all samples. Next, the first principal component (PC) was calculated for the data matrix formed by the genes in cluster 1, respectively cluster 2, which explained 65%, respectively 46%, of the variation of the data in the cluster. The sign of the PC was arbitrarily chosen such that the PC and the mean expression level of the cluster correlated positively. The resulting PCs of cluster 1 and 2 correlated negatively with Pearson correlation value $R = -0.2638$ and a *P*-value $P = 1.12 \times 10^{-5}$.

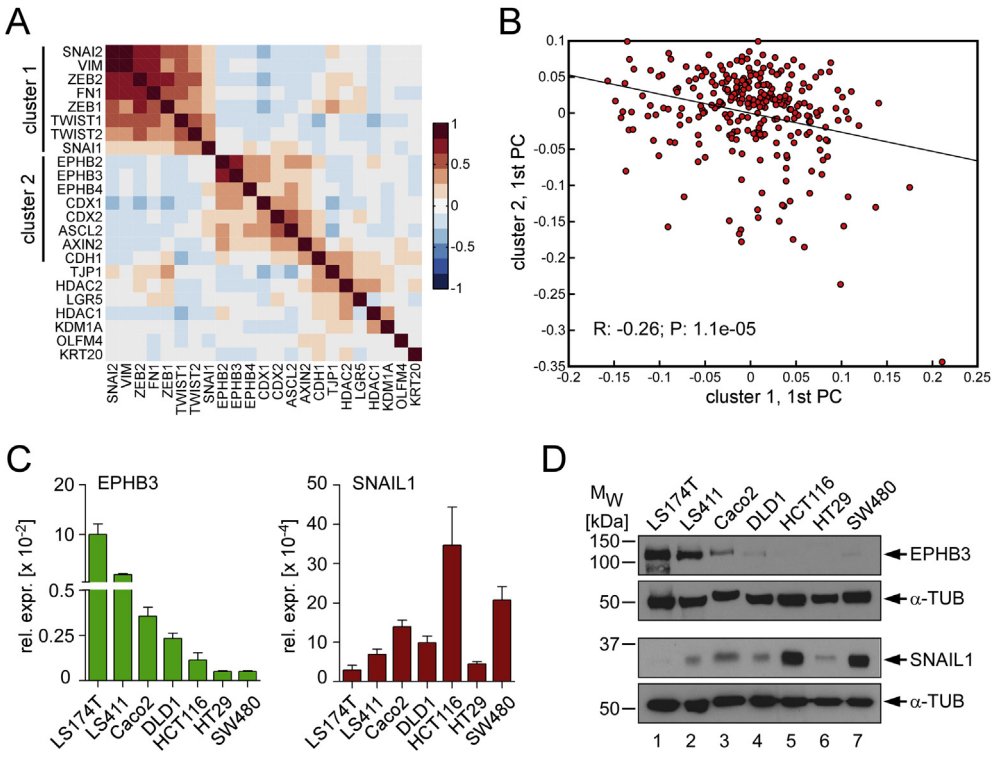

Figure 1 – Inverse expression of *EPHB3* and EMT inducers. (A) TCGA gene expression data were analyzed for pairwise correlated expression of *EPHB3* and EMT inducers. Color scale indicates the Pearson correlation coefficient as shown by the color bar. (B) Scatter plot of the first principal components for cluster 1 and cluster 2 as identified by the pairwise correlation analyses shown in (A). The straight line is the linear least-squares fit of the data with slope R: -0.2638 and a *P*-value $P = 1.12 \times 10^{-5}$. (C, D) qRT-PCR and Western Blot analyses of *EPHB3* and *SNAIL1* expression in human CRC cell lines. $n = 3$. α-TUBULIN (α-TUB) immunodetection to monitor for equal loading. M_W = molecular weight; rel. expr.: relative expression.

2.16. *Xenografts, tissue processing, histology and immunohistochemistry*

$Rag2^{-/-}\gamma c^{-/-}$ mice were purchased from a local stock (University of Freiburg animal facility). The animal protocol (G08-8) was approved by the Regierungspräsidium Freiburg (local animal committee Freiburg). Mice were injected subcutaneously with 5×10^6 LS174T CRC cell derivatives. Dox treatment was started on day 7 after injection to allow tumor establishment. Xenograft tumors ($n = 18$; six per group) were excised six days later, analyzed macroscopically, cut in half and processed via standard operating procedures (SOPs) for formalin-fixation and paraffin-embedding (FFPE). Serial sections of FFPE tissue specimens from all xenografts were stained by hematoxylin and eosin (HE) and by immunohistochemistry (EPHB3, E-Cadherin) according to SOPs. Antibodies used are listed in Supplementary Table S2.

2.17. *Statistical analysis*

Quantitative data are presented as means of at least three independent biological replicates with standard error of the mean (SEM). Statistical significance was determined by unpaired, two-tailed Student's *t*-test unless otherwise indicated. The corresponding symbols represent statistically significant changes with the following *p*-values: $^*P < 0.05$, $^{**}P < 0.01$, $^{***}P < 0.001$, $^{****}P < 0.0001$. ns: not significant.

3. Results

3.1. *Inversely correlated expression of* EPHB3 *and EMT inducers*

To examine a potential relationship between *EPHB3* expression and EMT we performed pairwise correlation analyses based on TCGA gene expression data for 270 samples of stage I-IV colon and rectum carcinomas (Cancer Genome Atlas, 2012). This analysis showed that inducers of EMT (e. g. *SNAIL1*, *SNAIL2*, *ZEB1*) and marker genes of EMT (*FN1*, *VIM*) formed a cluster of genes whose expression was positively correlated among each other (Figure 1A, cluster 1). Similarly, *EPHB3*, other EPHB receptor genes, the intestine-specific genes *CDX1* and *CDX2*, the ISC factor *ASCL2*, and the epithelial marker *CDH1* formed a distinct cluster of genes the expression of which was again positively correlated (Figure 1A, cluster 2). Intriguingly, the expression of the genes in cluster 1 and cluster 2 was clearly anti-correlated. To further examine the associations between the two groups of genes we carried out principal component (PC) analysis and calculated the first PCs for the data matrices formed by the genes in cluster 1 and cluster 2. Comparing the TCGA samples according to the resulting first PCs of the two clusters revealed a highly significant negative correlation (Pearson correlation value $R = -0.2638$, *P*-value of 1.12×10^{-5}; Figure 1B).

Next, we compared the expression of *EPHB3* and other intestinal epithelial genes with that of EMT inducers in a panel of colorectal cancer cell lines that carried various combinations of mutations in the TP53 tumor suppressor gene and components of Wnt/β-catenin, MAPK, PI3 kinase and TGFβ signaling pathways (Figure S1A) (Ahmed et al., 2013; Edlund et al., 2012; Mouradov et al., 2014; Rowan et al., 2000; Woodford-Richens et al., 2001). Irrespective of the particular genetic alterations in the different cell lines, we detected the inversely correlated expression of *EPHB3*, *EPHB2*, *EPHB4*, *CDX1* and *CDX2* on the one hand and the EMT inducers *SNAIL1*, *SNAIL2*, *ZEB1*, *ZEB2*, *TWIST1* and *TWIST2* on the other hand, also in this cohort of CRC cell lines (Figure 1C, D, Figure S1B, C). In case of *EPHB3*, low level expression was most consistently associated with elevated levels of *SNAIL1* (Figure 1C, D; Figure S1A–C). Interestingly, anti-parallel expression of *EPHB3* and *SNAIL1* was not only observed in CRC cell lines and tumor transcriptomes but also in cell lines from other cancers (Figure S1D). Taken together, these results suggest that *EPHB3* may be negatively regulated by the EMT inducer SNAIL1.

3.2. *Snail1 and SNAIL2 repress* EPHB3

EPHB3 expression is under critical control of a transcriptional enhancer centered around −2.3 kb upstream of the *EPHB3* transcriptional start site (Figure 2A) (Jägle et al., 2014). The *EPHB3* enhancer harbors binding sites for ETS factors, the Notch effector RBPJ and the TCF/LEF family member TCF7L2 (Hatzis et al., 2008; Jägle et al., 2014; Rodilla et al., 2009; van der Flier et al., 2009). In addition, the *EPHB3* enhancer has an E-box motif (Figure 2A). The *EPHB3* E-box could also serve as binding site for EMT inducers. Indeed, Snail1 and SNAIL2 bound to the *EPHB3* enhancer E-box *in vitro* and its mutation completely abolished this interaction (Figure 2B). Moreover, coexpression of murine Snail1 or human SNAIL2 repressed luciferase reporter activity driven by *EPHB3* upstream sequences which again was dependent on the *EPHB3* enhancer E-box (Figure 2C, D). In contrast, ZEB1 did not bind to the *EPHB3* enhancer E-box and had no effect on *EPHB3* reporter activity (Figure S2A, B), not even in the presence of its corepressor CtBP1 (Furusawa et al., 1999). Importantly, ZEB1 was fully functional when assayed at the *CDH1* promoter (Figure S2C). Thus, Snail1 and SNAIL2 are the best candidates for transcriptional repressors of *EPHB3*.

To analyze if Snail1 can downregulate endogenous *EPHB3*, we generated derivatives of LS174T cells that allowed for Dox-inducible expression of HA epitope-tagged mouse Snail1 (Snail1-HA) or human SNAIL1. Upon induction of Snail1-HA, LS174T cells changed their morphology and became more mesenchymal-like (Figure 2E). In time course experiments, *EPHB3* expression was diminished already within three hours after induction of Snail1-HA or SNAIL1 and was even further reduced at later time points (Figure 2F; Figure S3A). Expression of Snail1-HA in an additional CRC cell line (DLD1) yielded similar repressive effects on *EPHB3* (Figure S3B). Chromatin immunoprecipitation (ChIP) experiments showed that Snail1-HA binds to the endogenous *EPHB3* enhancer in LS174T and DLD1 cells (Figure 2G; Figure S3C) confirming that Snail1-HA directly targets *EPHB3*. Importantly, reduced expression of *EPHB3* is not due to impaired Wnt/β-catenin activity because β-catenin/TCF-dependent reporter expression and transcription of the Wnt/β-catenin target *AXIN2* were not diminished by Snail1-HA (Figure S4).

3.3. *Prolonged Snail1-HA expression hampers reactivation of* EPHB3

Snail1-HA-mediated *EPHB3* repression was further characterized by experiments in which Snail1-HA was transiently expressed for 24 h and 96 h. This was achieved by administration and subsequent wash out of Dox at the indicated time points (Figure 3A, C). As before, Snail1-HA induction led to *EPHB3* downregulation (Figure 3B, D). Washing out Dox after 24 h terminated Snail1-HA expression and *EPHB3* levels fully rebounded (Figure 3B). Similar observations were made with DLD1 cells (Figure S3D, E). Thus, repression of *EPHB3* at early time points is reversible and requires the continuous presence of Snail1-HA. In contrast, after long-term induction of Snail1-HA, *EPHB3* expression did not resume and remained low even upon shut-down of Snail1-HA expression (Figure 3C, D, conditions C, D). From this we conclude that prolonged expression of Snail1-HA can lead to conditions where repression of *EPHB3* becomes irreversible and persists even in the absence of Snail1-HA.

3.4. *Snail1 disables the* EPHB3 *enhancer to silence* EPHB3

To gain further insights into the mechanism of Snail1-mediated *EPHB3* repression and the potential cause of its long-term irreversibility we analyzed the impact of Snail1-HA on structural features of the *EPHB3* enhancer. By ChIP we examined the association of the *EPHB3* enhancer with Snail1-HA, the Wnt effector TCF7L2 and with monomethylated histone H3 lysine 4 (H3K4me1), a hallmark of poised and active enhancers (Calo and Wysocka, 2013). To our surprise, we found that 96 h post induction, Snail1-HA was no longer present at the *EPHB3* enhancer (Figure 4A) even though it had occupied the enhancer under conditions of short-term repression (see above, Figure 2G). Moreover, despite the apparent dissociation of Snail1-HA, TCF7L2 and the active histone mark H3K4me1 were also absent from the *EPHB3* enhancer in cells treated with Dox for 96 h (Figure 4B, C). A displacement of TCF7L2 by Snail1-HA was also observed in DLD1 cells (Figure S3C). To further analyze the impact of Snail1-HA on chromatin accessibility of the *EPHB3* enhancer we used formaldehyde-assisted isolation of regulatory elements (FAIRE) (Giresi et al., 2007). Thereby, the open chromatin state at the *EPHB3* enhancer was found to be only slightly impaired 24 h after Dox addition. However, it was completely abolished 96 h after Snail1-HA induction (Figure 4D). Seemingly, Snail1-HA triggers a series of processes that lead to the erasure of a critical histone mark and the generation of a chromatin state that precludes transcription factor binding (including that of Snail1-HA). Thus, Snail1-HA completely disables the *EPHB3* enhancer which likely explains not only *EPHB3* repression but also its persistence even upon shut-down of Snail1-HA expression.

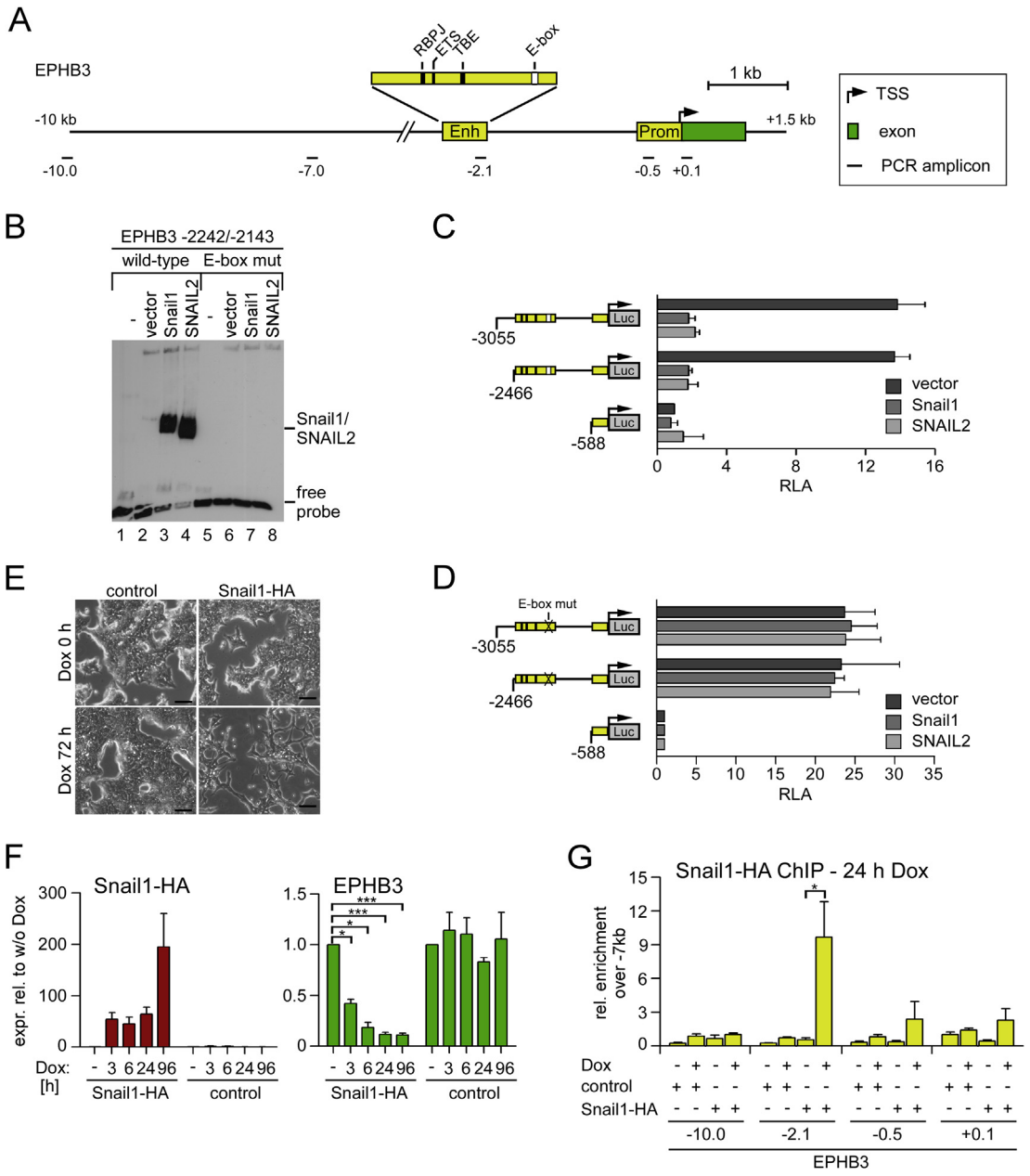

Figure 2 – *EPHB3* is a direct target gene of Snail1. (A) Schematic representation of the *EPHB3* 5'-flanking region showing the location of the *EPHB3* enhancer with its binding motifs for RBPJ and ETS family members, the TCF/LEF binding element (TBE) and an E-box. Positions of primer pairs used for ChIP and FAIRE analyses are also indicated. Enh: enhancer; Prom: Promoter; TSS: transcriptional start site. (B) EMSA demonstrating binding of Snail1 and SNAIL2 to the *EPHB3* enhancer E-box *in vitro*. (C,D) Effect of Snail1 and SNAIL2 on *EPHB3*-driven luciferase reporter activity in LS174T cells. The grey box indicates the enhancer region. Binding sites for RBPJ and ETS factors, the TBE and the E-box are indicated. RLA: relative luciferase activity. $n = 3$. The E-box was mutated in (D). (E) Representative pictures of derivatives of LS174T cells 72 h after Snail1-HA induction. Scale bar: 100 μm. (F) qRT-PCR analyses of *Snail1-HA* and *EPHB3* in derivatives of LS174T cells. Expression (expr.) levels are shown as values relative (rel.) to controls without (w/o) Dox treatment. $n = 3$, paired, two-tailed Student's *t*-test. (G) ChIP analyses of Snail1-HA occupancy at the *EPHB3* locus in derivatives of LS174T cells 24 h after Snail1-HA induction. $n = 3$.

3.5. *Snail1 competes with ASCL2 for binding to the* EPHB3 *enhancer*

Next, we investigated the molecular mechanisms whereby Snail1-HA acutely represses *EPHB3* and tested whether Snail1-HA competes with ASCL2 for binding to the *EPHB3* enhancer E-box. EMSAs were performed in which amounts of ASCL2-HA were kept constant while adding increasing amounts of Snail1-HA. Thereby, Snail1-HA gradually displaced ASCL2-HA from the *EPHB3* probe (Figure 5A). Consistent with this competitive displacement, Snail1-HA neutralized ASCL2-HA-mediated stimulation of *EPHB3* luciferase reporter activity in a dose-dependent manner (Figure 5B). Moreover, ChIP showed that Snail1-HA induction displaced endogenous

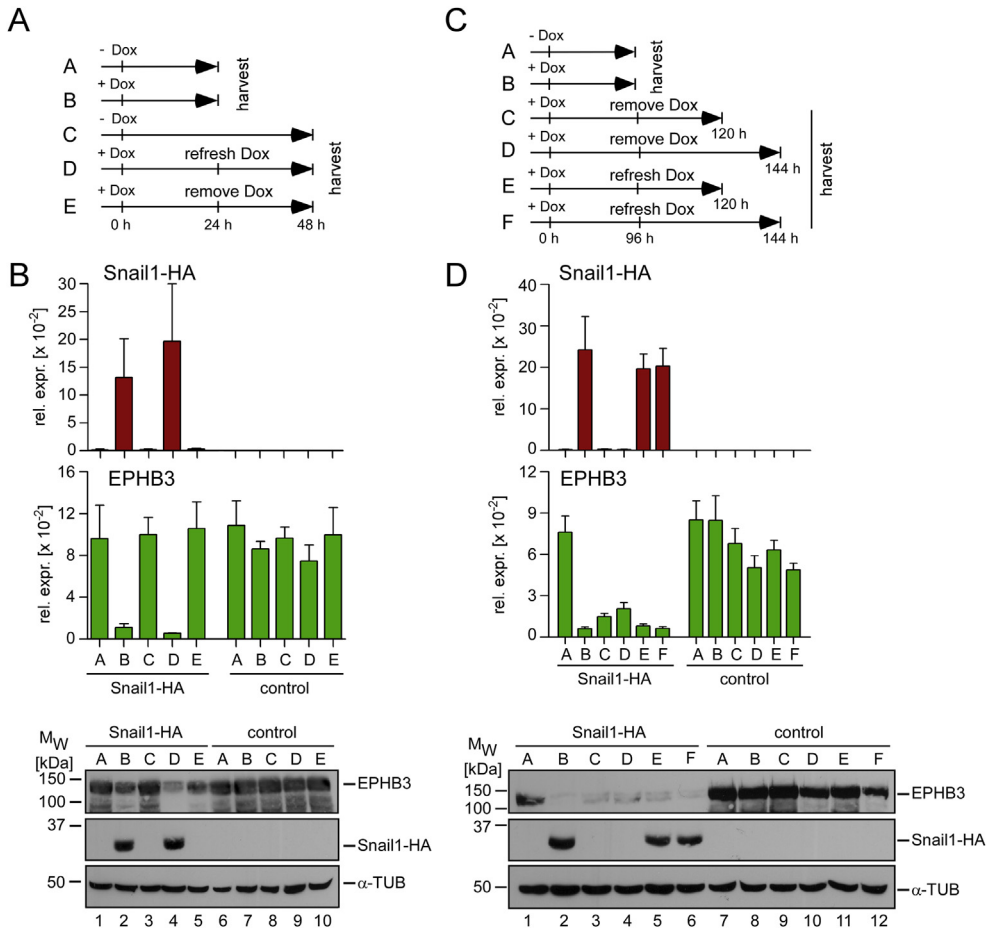

Figure 3 – Long-term expression of Snail1-HA hampers reactivation of *EPHB3*. (A) Experimental set-up for wash-out experiments shown in (B). (B) Expression analyses of Snail1-HA and EPHB3 by qRT-PCR (top) and Western Blot (bottom) in LS174T CRC cell derivatives. $n = 3$. α-TUBULIN (α-TUB) immunodetection to monitor for equal loading. M_W = molecular weight; rel. expr.: relative expression. (C) Experimental set-up for wash-out experiments shown in (D). (D) Expression analyses of Snail1-HA and EPHB3 by qRT-PCR (top) and Western Blot (bottom) in LS174T CRC cell derivatives. $n = 3$. α-TUBULIN (α-TUB) immunodetection to monitor for equal loading. M_W = molecular weight; rel. expr.: relative expression.

ASCL2 from the *EPHB3* enhancer region (Figure 5C). Overall this shows that Snail1-HA counteracts ASCL2 binding to the *EPHB3* enhancer E-box and strongly suggests that this contributes to the transcriptional shut-down of *EPHB3*.

3.6. *The SNAG domain is required for Snail1-mediated* EPHB3 *repression*

SNAIL1/SNAIL2 can repress target genes not only by competitive displacement of transcription factors but also in concert with corepressor complexes that interact with the N-terminal SNAG domain (Lin et al., 2010a, 2010b; von Burstin et al., 2009). To investigate if corepressor complexes play a role in Snail1-mediated *EPHB3* repression we generated a Snail1-HA mutant lacking the SNAG domain. *In vitro*, Snail1-HA-ΔSNAG bound to the *EPHB3* enhancer E-box (Figure 6A) but repression of *EPHB3* luciferase reporter constructs was impaired (Figure S5A). To examine its impact on the expression of endogenous *EPHB3*, we established LS174T cells with Dox-inducible expression of Snail1-HA-ΔSNAG. Both mutant and full-length Snail1-HA were expressed at similar levels (Figure 6B, Figure S5B) and bound to the *EPHB3* enhancer region although enrichment of Snail1-HA-ΔSNAG was reduced (Figure 5C). However, Snail1-HA-ΔSNAG was unable to downregulate *EPHB3*, *CDH1* or the intestine-specific genes *KRT20* and *CDX2* (Figure 6B, Figure S5C). Importantly, Snail1-HA-ΔSNAG could not expel ASCL2, TCF7L2 and the co-activator p300 from the *EPHB3* enhancer (Figure 6C). Thus, the SNAG domain is essential for displacement of activator proteins and for *EPHB3* repression.

3.7. *Snail1 engages HDACs and LSD1 to silence* EPHB3

SNAIL1/SNAIL2 use the SNAG domain to interact with several corepressor complexes that harbor among others histone-modifying enzymes (Lin et al., 2010a, 2010b; von Burstin et al., 2009). By co-immunoprecipitation we confirmed that HDAC1, HDAC2 and the lysine demethylase LSD1 form complexes with Snail1-HA depending on the SNAG domain (Figure S6A). In order to determine if any of the chromatin-modifying Snail1-HA interactors are involved in *EPHB3*

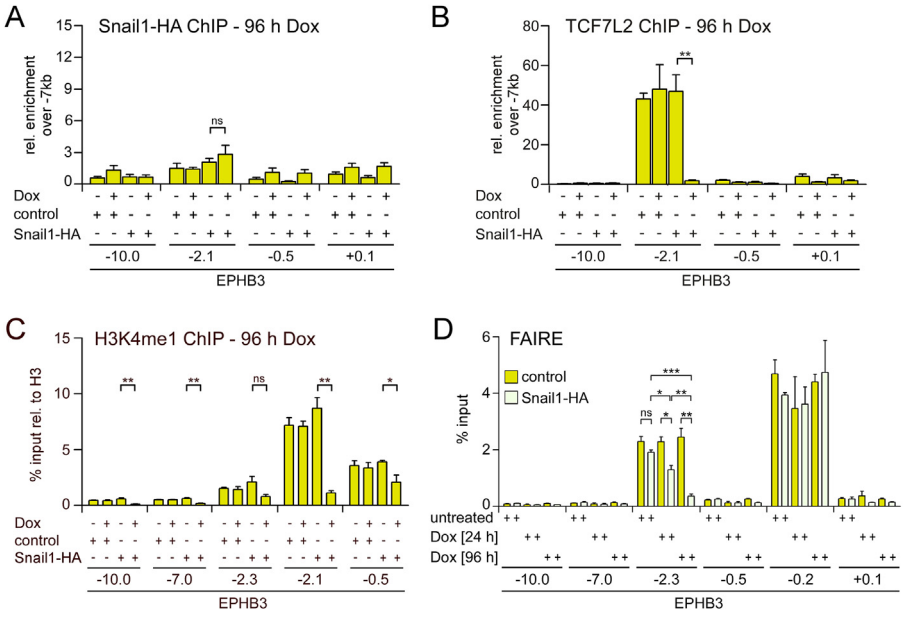

Figure 4 – Snail1-HA completely disables the *EPHB3* enhancer. (A–C) ChIP analyses of Snail1-HA (A), TCF7L2 (B) and H3K4me1 (C) occupancy at the *EPHB3* locus in derivatives of LS174T cells 96 h after Snail1-HA induction. $n \geq 3$. (D) FAIRE analysis of chromatin structure at the *EPHB3* locus in LS174T CRC cell derivatives stably transduced with Dox-inducible retroviral control or Snail1-HA expression vectors. Dox was added for 24 h or 96 h. FAIRE-DNA was analyzed by qPCR. Data were calculated as percent input. $n = 3$.

repression, we analyzed changes in histone modifications following Snail1-HA induction. The repressive histone mark H3K27me3 is a signature of PRC2 activity. However, H3K27me3 levels at the *EPHB3* locus were low and did not increase in the presence of Snail1-HA (Figure S6B). Therefore, we excluded PRC2 from further analyses. In contrast, induction of Snail1-HA but not of Snail1-HA-ΔSNAG, greatly reduced H3 acetylation (H3ac) and H3K4 methylation levels (H3K4me3) at multiple positions of the *EPHB3* upstream region (Figure 7A; Figure S6C) suggesting that HDACs and histone demethylases are involved in *EPHB3* repression.

We first focused on HDACs and detected significantly increased HDAC1 occupancy at multiple positions around the *EPHB3* gene when Snail1-HA was induced (Figure 7B) indicating that corepressor complexes containing HDAC1 were recruited by Snail1-HA and spread across the entire *EPHB3* locus. Importantly, the induction of Snail1-HA-ΔSNAG did not lead to recruitment of HDAC1 (Figure S6C), confirming specificity and Snail1-dependence of HDAC1 recruitment. Furthermore, to address their functional importance in *EPHB3* repression, we performed individual and combinatorial knockdown of several HDACs. For this we used SW480 CRC cells with low levels of endogenous *EPHB3* but high amounts of SNAIL1/SNAIL2. In fact, specifically the combined knockdown of HDAC1 and HDAC2 significantly increased *EPHB3* expression whereas various combinations involving knockdown of HDAC3, HDAC7 and HDAC8 did not (Figure 7C and Figure S6D). Furthermore, the class I HDAC inhibitor MS275 interfered with Snail1-mediated *EPHB3* repression in LS174T and HT29 cells stably transduced with a Dox-inducible Snail1-HA expression vector (Figure S6E,F).

Next, we addressed the role of the histone demethylase LSD1 in *EPHB3* repression. LSD1 was enriched at the *EPHB3* enhancer region (Figure 7D) but we detected LSD1 at the *EPHB3* enhancer already prior to Snail1-HA induction. Possibly, LSD1 functions at *EPHB3* as part of both coactivator and corepressor complexes as in other cases (Metzger et al., 2005; Yatim et al., 2012). Importantly, pharmacological inhibition of LSD1 by TCP impaired *EPHB3* downregulation by Snail1-HA (Figure 7E and Figure S6G). Taken together, we conclude that Snail1-HA engages HDACs and LSD1 as corepressors to disable the *EPHB3* enhancer and to silence *EPHB3*.

3.8. *Snail1 induces an EMT but interferes with features of intestinal epithelial stem cells*

SNAIL1/SNAIL2 are potent inducers of EMT in various cellular systems (Peinado et al., 2007). In fact, Snail1-HA not only repressed *EPHB3* but also induced a complete EMT in LS174T cells as indicated by upregulation of the mesenchymal markers *ZEB1* and *FN1*, downregulation of the epithelial marker *CDH1*, enhanced migration, more invasive growth and reduced population dynamics (Figure S7). This was accompanied by Snail1-HA-induced upregulation of the CDK inhibitor CDKN1A/p21^{CIP1} (Figure S7C). Snail1-HA-induced morphological changes were completely blocked by MS275 or TCP (Figure S7F). Furthermore, Snail1-HA-ΔSNAG could not impair proliferation, enhance migration or the formation of invasive sprouts in spheroids of LS174T cells (Figure S7B,D,E) confirming that chromatin-modifying corepressors are integral to the Snail1-induced EMT.

It was proposed that EMT confers properties of stemness. Interestingly, LS174T cells already bear characteristics of ISCs (van de Wetering et al., 2002) which are thought to be the cells of origin in CRC (Barker et al., 2009). Therefore, we were curious to determine the effects of Snail1-HA on the

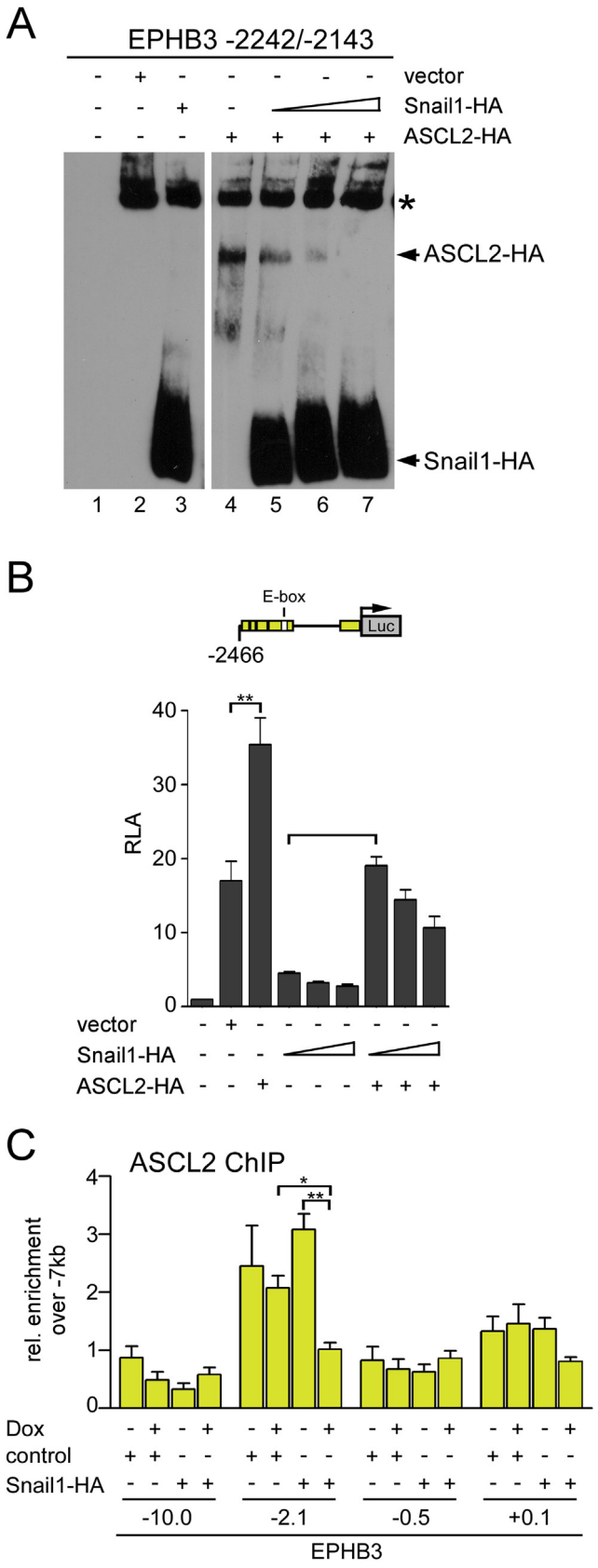

Figure 5 – ASCL2 and Snail1 compete for binding to the *EPHB3* E-Box. (A) EMSA with ASCL2-HA and Snail1-HA and a probe containing the *EPHB3* enhancer E-box. Asterisk: non-specific band. (B) Activity of an *EPHB3*-driven luciferase reporter upon expression of ASCL2-HA and Snail1-HA as shown. The grey box indicates the enhancer region. Binding sites for RBPJ and ETS factors, the TBE and the E-box are indicated. RLA: relative luciferase activity. $n \geq 4$. (C) ChIP analyses of ASCL2 occupancy at *EPHB3* in derivatives of LS174T cells. $n = 3$.

expression of marker genes characteristic for intestinal differentiation and ISCs and on sphere-forming capacity which is an accepted surrogate assay to gauge stemness properties *in vitro* (O'Brien et al., 2012). Time-course experiments revealed that marker genes for intestinal identity and differentiation (*CDX1*, *CDX2*, *KRT20*) (Dalerba et al., 2011; Stringer et al., 2012; Verzi et al., 2011), markers of ISCs (*ASCL2*, *LGR5*, *OLFM4*) (Itzkovitz et al., 2012; Munoz et al., 2012) and the two other intestinal EPHB family members *EPHB2* and *EPHB4* were downregulated after induction of Snail1-HA (Figure 8A; Figure S8), albeit with different temporal profiles. Of note, these results are consistent with gene expression analyses of the TCGA RNA-Seq data which had already highlighted that expression of *EPHB2*, *EPHB4*, *KRT20*, *CDX1*, *CDX2 and ASCL2* is anti-correlated perhaps not strictly with *SNAIL1* but with EMT inducers in a more general way (see Figure 1A). Furthermore, despite a modest upregulation of some genes characterizing putative tumor initiating cells after extended periods of Snail1-HA expression (Figure S9), Snail1-HA expression resulted in impaired self-renewal capacity as shown by a serial limiting dilution/sphere formation assay (Figure 8B). Overall, the observed gene expression changes and the functional evidence indicate that in our cellular system Snail1-HA broadly interferes with features of intestinal epithelial stem cells.

3.9. *Sustained expression of EPHB3 interferes with Snail1-induced EMT*

EPHB3 was downregulated much faster by Snail1-HA than *CDH1*. EPHB3 is known to affect E-Cadherin function (Chiu et al., 2009; Cortina et al., 2007). We wondered about the significance of rapid *EPHB3* repression and asked whether sustained expression of EPHB3 could counteract Snail1-induced EMT. For this, we additionally introduced into LS174T cells with Dox-inducible Snail1-HA expression a lentiviral vector for constitutive, Snail1-independent *EPHB3* expression (Figure 9A). As expected, induction of Snail1-HA in these cells reduced overall amounts of *EPHB3* by repressing the endogenous gene but the remaining levels derived from lentivirally-encoded *EPHB3* were similar to those of control cells (Figure 9B, lanes 3 and 4). Note, that LS174T cells express EPHB receptor ligands that are additionally upregulated by Snail1-HA (Figure S10). Therefore, we presume that the EPHB3 receptors are active under our experimental conditions. The impact of continuous presence of EPHB3 on EMT was analyzed by its effects on cell motility and invasion. Interestingly, Snail1-HA-induced migration was reduced when EPHB3 expression was maintained (Figure 9C). Moreover, aggregates formed by cells expressing both Snail1-HA and EPHB3 also tended to extend fewer sprouts per spheroid in collagen I matrices and the remaining sprouts were significantly shorter compared to cells expressing only Snail1-HA

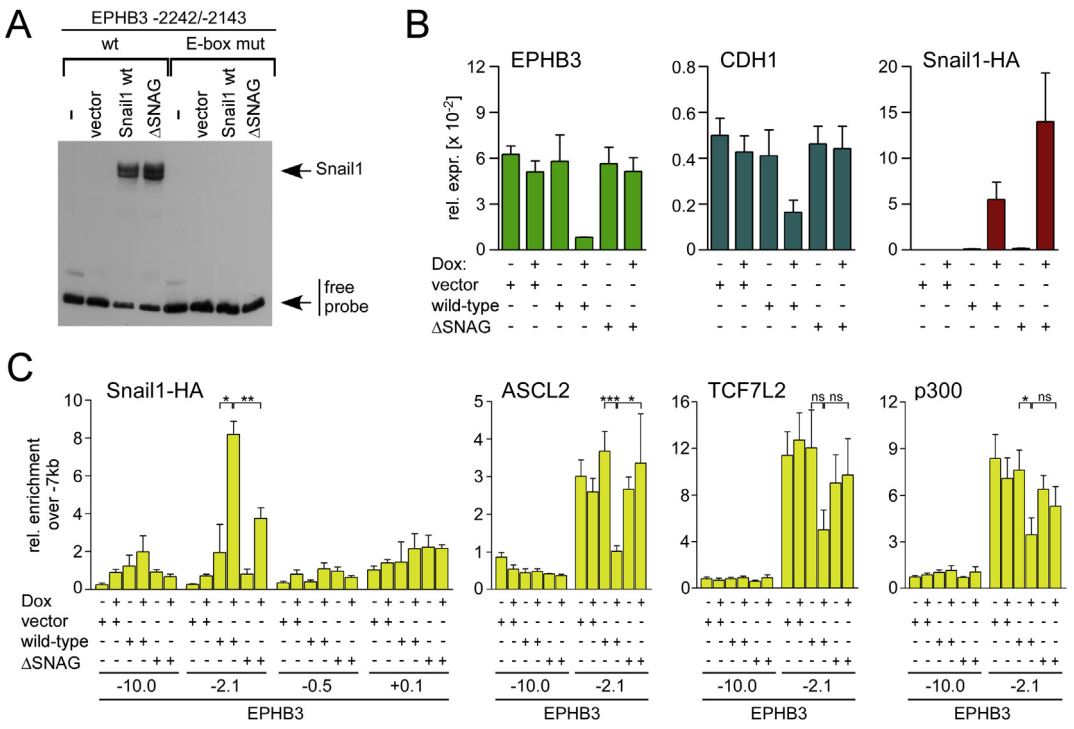

Figure 6 – Repression of *EPHB3* requires the SNAG-domain. (A) EMSA with wild-type Snail1-HA (wt) and Snail1-HA-ΔSNAG and the indicated *EPHB3* probes. (B) qRT-PCR analyzing relative expression (rel. expr.) of the indicated genes in derivatives of LS174T cells. $n = 3$. (C) ChIP analyses of *EPHB3* occupancy by the indicated factors in derivatives of LS174T cells. $n \geq 3$.

(Figure 9D,E). Clearly, sustained expression of EPHB3 impairs EMT induction by Snail1-HA.

To examine whether the phenotypic changes observed *in vitro* also occur *in vivo*, we generated xenograft tumors with LS174T control cells ($n = 6$), the LS174T-Snail1-HA single transgenic ($n = 6$) and the LS174T-Snail1-HA/EPHB3 double transgenic cell lines ($n = 6$). The different cell lines were injected subcutaneously into the flanks of immunodeficient mice and tumors were allowed to form for 7 days. At this time point the mice received Dox to induce expression of Snail1-HA and tumors were allowed to grow for another 6 days before excision and examination. No difference with respect to the size of tumors formed by control, single transgenic or double transgenic cells was seen (Figure S11). HE staining of control xenograft tumors revealed a compact architecture with palisade orientation of tumor cells around fibrovascular cores, large areas of apoptosis and an encapsulated tumor mass (Figures 10 and S12, left). Tumor cells of control xenografts expressed membranous EPHB3 and E-Cadherin. In contrast, LS174T-Snail1-HA xenografts showed markedly altered architecture and cellular organization which was characterized by abrogated tumor cell palisading, reduced stromal compaction, regional loss of tumor encapsulation and the occurrence of areas with tumor cells displaying a migratory phenotype (Figures 10 and S12, center). This was accompanied by downregulation or loss of EPHB3 and E-Cadherin expression in clusters of tumor cells which also showed detachment from the main tumor mass and were surrounded by stromal cells at the invasion front. In xenografts formed by Snail1-HA/EPHB3 double transgenic cells, the patterns and levels of EPHB3 expression resembled controls. Moreover, experimentally preserved expression of EPHB3 attenuated the Snail1-HA-induced phenotype as indicated by continued E-Cadherin expression and by tumor architecture and encapsulation that approximated control xenografts (Figures 10 and S12, right). Taken together, EPHB3 appears to antagonize Snail1-HA also *in vivo*.

4. Discussion

EMT-induced changes in cellular properties play important roles in developmental processes but also in physiological responses to tissue injury (Kalluri and Weinberg, 2009). EMT also appears to facilitate tumor cell invasion and dissemination in many different cancers (Kalluri and Weinberg, 2009) and there is growing evidence that EMT is of critical importance in CRC as well (De Sousa et al., 2013; Hwang et al., 2014, 2011; Loboda et al., 2011; Shioiri et al., 2006; Wang et al., 2010). The results of our expression profiling in CRC cell lines and the analysis of the TCGA gene expression data are in agreement with these findings and provide additional evidence that EMT-regulating transcription factors are aberrantly expressed in CRC and antagonize epithelial cell characteristics. Our study shows that expression of SNAIL1 in CRC cells causes the deregulation of several intestinal epithelial genes previously unknown to be affected by EMT. This provides further insight into the complexity and the profound molecular changes that accompany EMT.

EPHB receptors exert important tumor suppressive functions in CRC (Batlle et al., 2005; Chiu et al., 2009). However, at the transition from non-invasive adenomas to invasive

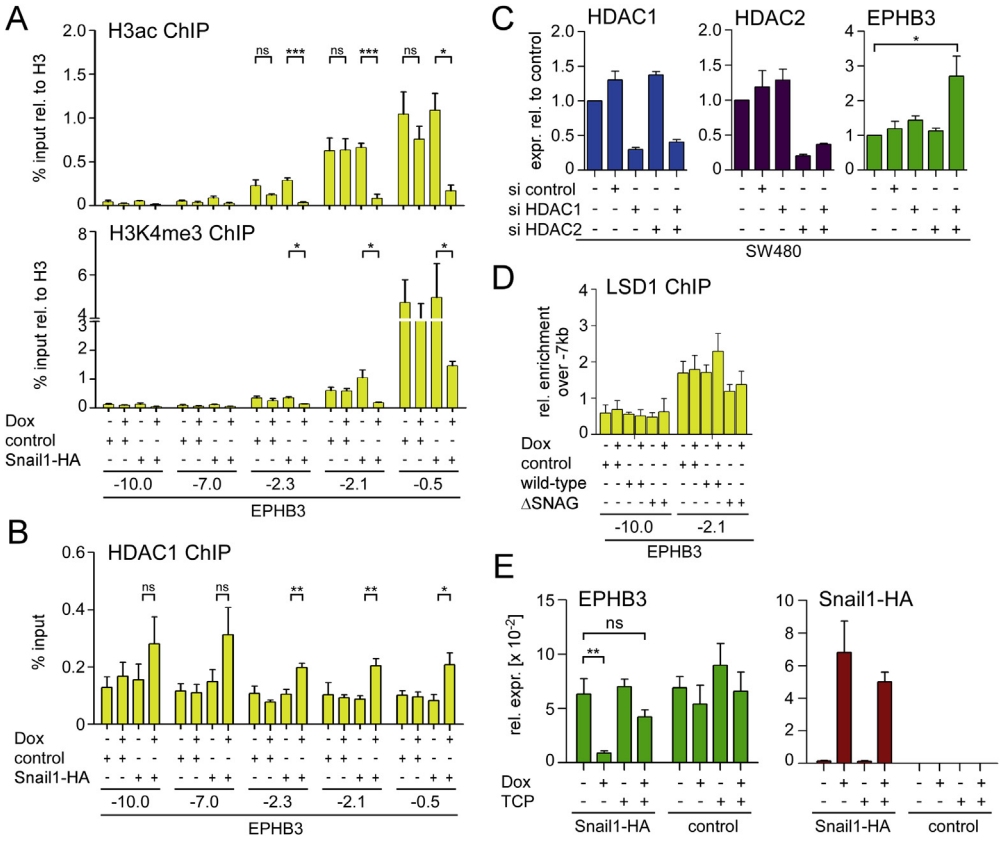

Figure 7 – Snail1-HA engages HDACs and LSD1 to repress *EPHB3*. (A,B) ChIP analyses of H3ac, H3K4me3 (A) and HDAC1 occupancy (B) in derivatives of LS174T cells. $n \geq 3$. (C) qRT-PCR analyzing *HDAC1*, *HDAC2* and *EPHB3* expression after knockdown of HDAC1 and/or HDAC2 in SW480 cells. Expression (expr.) levels are shown as values relative (rel.) to control. $n = 3$. (D) ChIP analyses of LSD1 occupancy in derivatives of LS174T cells. $n \geq 3$. (E) qRT-PCR analyzing relative expression (rel. expr.) of *EPHB3* and *Snail1-HA* in derivatives of LS174T cells treated with Dox and TCP. $n = 4$.

carcinoma states EPHB receptors are frequently transcriptionally downregulated (Batlle et al., 2005; Chiu et al., 2009; Rönsch et al., 2011). Here, we describe *EPHB3* as a novel and direct target gene of SNAIL1/SNAIL2 transcription factors and uncover a mechanism whereby *EPHB3* expression can be incapacitated in tumorigenesis. Based on our findings we propose the following model for Snail1-mediated inactivation of *EPHB3* (Figure 11). In *EPHB3* expressing cells a multifactorial transcription factor complex assembles at the *EPHB3* enhancer. Upon acute induction of EMT, Snail1 disables this enhancer by expelling the transcription activator proteins and by triggering an HDAC- and LSD1-mediated removal of activating chromatin marks. Ultimately, Snail1 itself appears to dissociate from the *EPHB3* enhancer leaving behind completely condensed, inactive chromatin.

A crucial aspect in *EPHB3* enhancer decommissioning appears to be the competitive displacement of ASCL2 from a common E-box binding site. This process could additionally be facilitated by the Snail1-induced transitory downregulation of ASCL2. The *EPHB3* gene thus provides an additional example where Snail1 antagonizes a key developmental regulator from the bHLH family of transcription factors (Soleimani et al., 2012). To our knowledge, this is the first description of a competition between an aberrantly expressed EMT inducer and a tissue-specific activator during tumorigenesis. In view of the widespread role of bHLH factors in organ development and tissue homeostasis this scenario might constitute a more common paradigm for the deregulation of tumor-relevant genes. It would be interesting to further explore its importance also at other target genes of EMT inducers.

In addition to the displacement of ASCL2, Snail1 engages HDACs and LSD1 to expel TCF7L2, p300 and probably other activators from the *EPHB3* locus (Figure 11). We previously reported that the inactive *EPHB3* locus shows a depletion of active histone marks and provided evidence that class I HDACs are involved in its repression (Rönsch et al., 2011). Here, we identified Snail1 as a DNA-binding factor that can recruit HDACs to the *EPHB3* locus to promote the loss of active histone marks. While HDACs seemingly are attracted to the *EPHB3* locus by Snail1, LSD1 turned out to reside at the *EPHB3* locus also in its absence. As in other cases (Metzger et al., 2005; Yatim et al., 2012), LSD1 may undergo a switch from coactivator to corepressor upon occupancy of the *EPHB3* locus by Snail1. Alternatively, there could be an exchange of LSD1-containing transcription complexes that escaped detection by ChIP. Irrespective of this, detailed knowledge about the context-dependent interaction partners and corepressors of SNAIL1 is of crucial importance also from a therapeutic perspective. Transcription factors like SNAIL1 are poor drug targets whereas HDACs and LSD1 are druggable

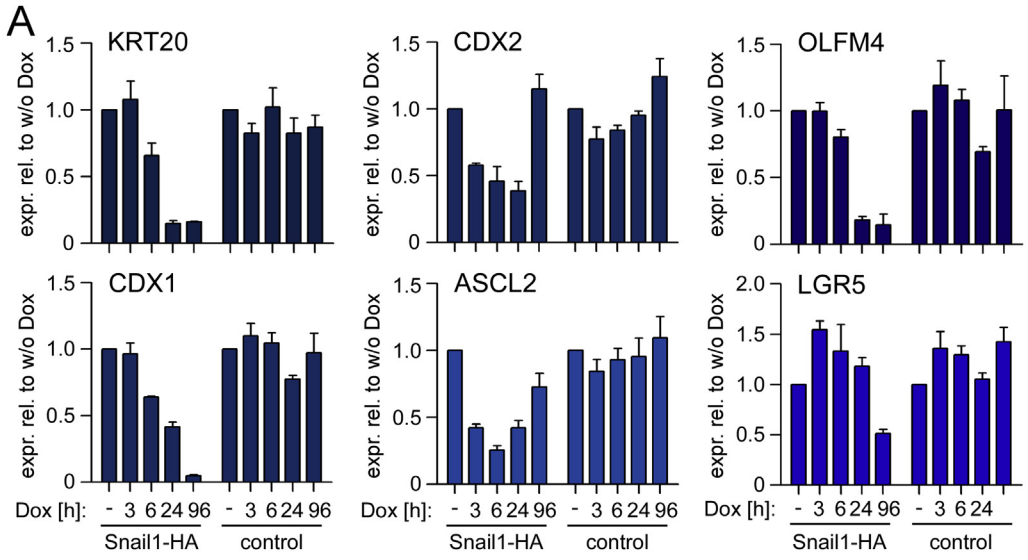

B

		Frequency of sphere forming units *in vitro*	
		1st generation	2nd generation
control	- Dox	1 in 16.6 (10.8 - 25.8)	1 in 5.0 (3.6 - 7.0)
	+Dox [0.1 µg/ml]	1 in 8.2 (5.6 - 11.6)	1 in 4.0 (2.9 - 5.6)
Snail1- HA	- Dox	1 in 2.4 (1.9 - 3.5)	1 in 5.5 (3.9 - 7.8) ***
	+Dox [0.1 µg/ml]	1 in 10.2 (6.9 - 15.2)	1 in 13.0 (8.6 - 19.0)

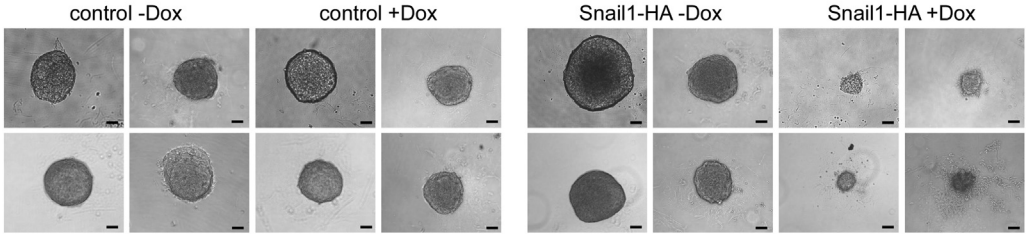

Figure 8 – Snail1-HA expression interferes with marker gene expression of intestinal epithelial stem cells and self-renewal capacity. (A) qRT-PCR analyses of the genes shown in derivatives of LS174T cells. Expression (expr.) levels are shown as values relative (rel.) to controls without (w/o) Dox treatment. $n \geq 3$. (B) Sphere formation capacity and serial limiting dilution analysis to assess stem cell properties of LS174T CRC cell derivatives stably transduced with Dox-inducible retroviral control or Snail1-HA expression vectors ($n = 4$; numbers in parentheses: upper and lower 95% confidence intervals for the frequency of sphere forming units). chi-squared *test*. Representative pictures of spheres 7 days after plating are shown. Scale bar: 100 µm.

enzymes and thus provide a window of opportunity to interfere with SNAIL1-induced repression of *EPHB3* and other epithelial genes.

Prolonged Snail1-HA expression eventually led to its own release from the *EPHB3* enhancer. The apparent self-eviction of Snail1-HA might be consequential to the removal of active histone marks and the ensuing closure of *EPHB3* enhancer chromatin. The observation that *EPHB3* repression did not require permanent binding of Snail1 and was upheld even upon shut-down of Snail1-HA has important implications. Thus, it may not be possible to restore *EPHB3* expression just by targeting Snail1. Moreover, if this hit-and-run mechanism applies more frequently, the number of genes afflicted by Snail1-induced silencing may be grossly underestimated upon completion of EMT.

Mechanistically, transcriptional repression by Snail1 so far has best been characterized at the *CDH1* promoter but concentrated on Snail1 corepressors that target chromatin. The triple attack on *EPHB3* control mechanisms involving activator deprivation by *ASCL2* downregulation, competition for a common binding site and the participation of histone modifiers is a novel aspect and could explain the rapid loss of *EPHB3* expression that considerably preceded *CDH1* downregulation. It is tempting to speculate that also other Snail1 target genes are regulated in a similarly complex fashion. In support of this, not only *ASCL2* but also the transcriptional regulators *CDX1*, *CDX2* (this study) and *VDR* (Pena et al., 2005) are negatively affected by Snail1, and their deregulation could contribute to gradually spreading changes in epithelial gene expression programs. This could explain the different kinetics

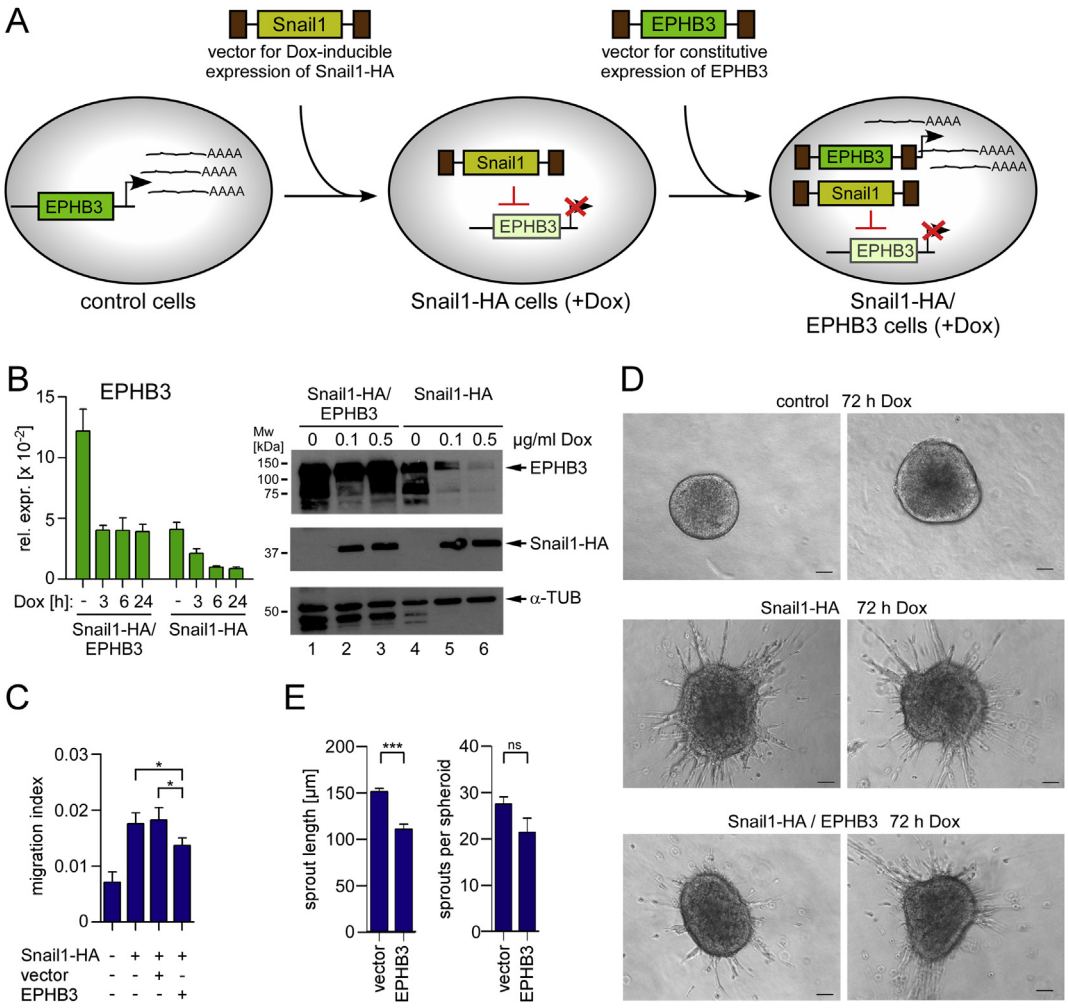

Figure 9 – Sustained expression of EPHB3 interferes with Snail1-HA-induced EMT. (A) Scheme illustrating the construction of LS174T CRC cell derivatives. In a first step, LS174T cells were tranduced with a retroviral vector for Dox-inducible expression of Snail1-HA, yielding Snail1-HA cells. In a second step, the Snail1-HA cells were transduced with a lentiviral vector for constitutive expression of EPHB3 that is not affected by Snail1-HA (Snail1-HA/EPHB3 cells). The situation in the presence of Dox is depicted. (B) qRT-PCR and Western Blot analyzing EPHB3 expression in derivatives of LS174T cells. $n = 4$; α-TUBULIN (α-TUB) immunodetection to monitor for equal loading. M_W = molecular weight; rel. expr.: relative expression. (C) Analyses of migration of LS174T cell derivatives. $n = 9$, paired, two-tailed Student's t-test. (D) 3D growth of LS174T cell derivatives. Scale bar: 100 µm. (E) Quantification of sprout length and number formed by LS174T cell derivatives. $n = 3$; 4 to 15 spheroids per biological replicate for each condition.

of transcriptional responses of Snail1 target genes and thereby also the perplexingly slow progress of EMT.

The *EPHB3* enhancer seemingly plays a central role in driving *EPHB3* expression in different cell-types within the intestinal epithelium and inactivation of the enhancer appears to be the key event in *EPHB3* secondary silencing (Jägle et al., 2014). Our previous studies identified defective Notch signaling as one of the causes that can lead to *EPHB3* enhancer decommissioning. However, defective Notch signaling could explain *EPHB3* secondary silencing only in a subset of CRC cells (Jägle et al., 2014). In this study we show that the induction of EMT and Snail1 represent an alternative way to disable the *EPHB3* enhancer and thereby silence *EPHB3*. That CRC cells can employ multiple strategies for *EPHB3* enhancer decommissioning is in good agreement with the existence of several distinct subtypes of colorectal tumors which can be distinguished based on their molecular features (Cancer Genome Atlas, 2012; Sadanandam et al., 2013). The particular design of the *EPHB3* enhancer which functions as a signal integrator element that receives input from multiple signaling pathways and transcription factors likely makes this regulatory element especially vulnerable to tumor-associated disturbances in cellular signaling networks and explains the recurrent inactivation of the *EPHB3* tumor suppressor in a large fraction of colorectal carcinomas (Batlle et al., 2005; Chiu et al., 2009; Rönsch et al., 2011).

Our comparative and time-dependent gene expression analyses showed that Snail1 had a widespread and profound impact on LS174T CRC cells which were seminal for the discovery and characterization of ISCs (van de Wetering et al., 2002). Beyond its effects on EPHB receptors, expression of SNAIL1 induced the downregulation of several other genes with critical functions in stem cell maintenance and

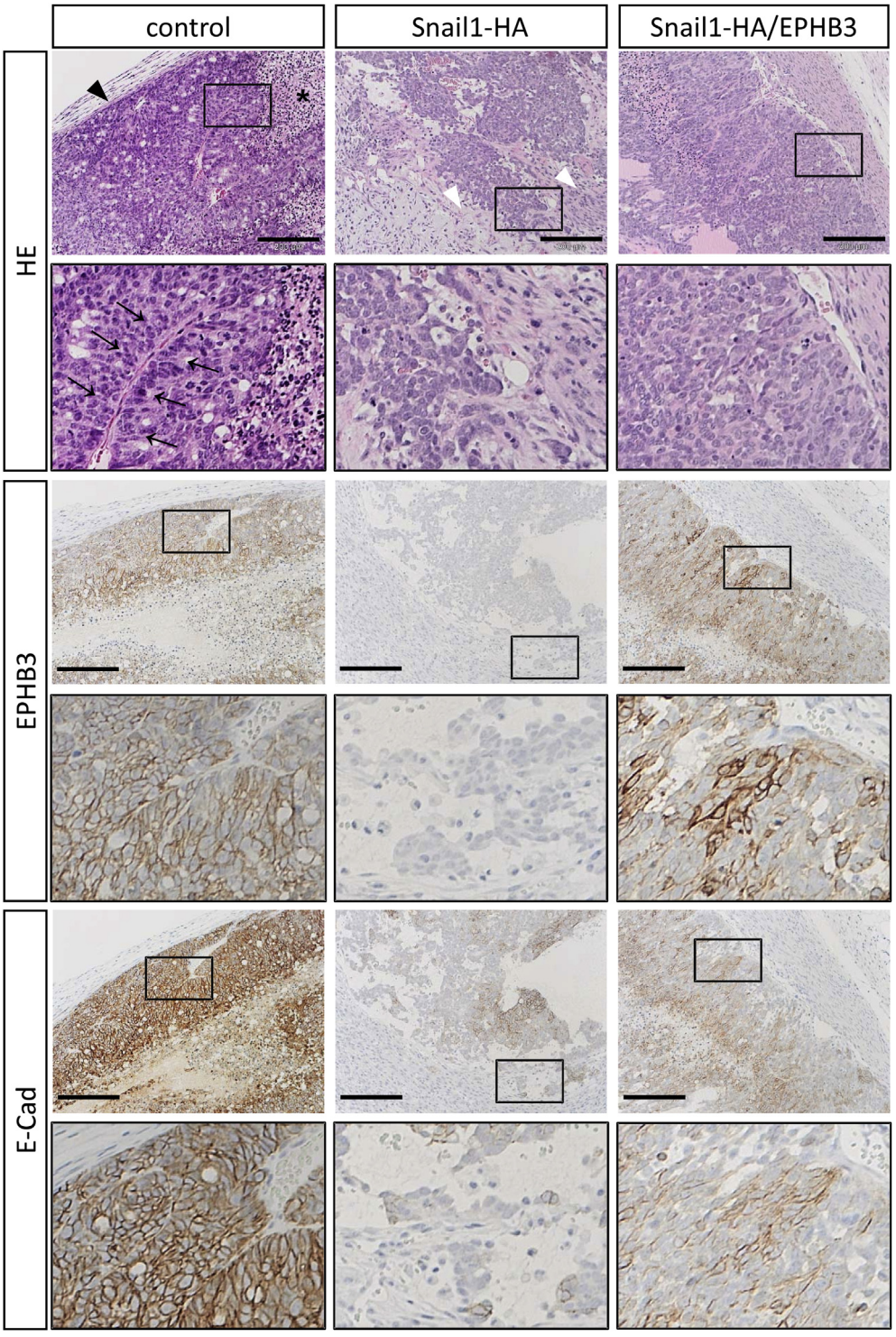

Figure 10 – EPHB3 counteracts Snail1-HA-induced EMT *in vivo*. Representative images of serial sections of xenograft tumors formed by LS174T control cells or derivatives expressing Snail1-HA and Snail1-HA in the continuous presence of EPHB3 (Snail1-HA/EPHB3) in Dox-treated Rag2$^{-/-}\gamma c^{-/-}$ mice. Upper panels: HE stainings. Lower panels: immunohistochemical analyses of EPHB3 and E-Cadherin (E-Cad). 10-fold enlargements of boxed areas are shown below the corresponding micrographs. Scale bars: 200 μm. Asterisk: apoptotic area. Black arrowhead and arrows in controls: sharply demarcated tumor margin and nuclear palisading around fibrovascular cores, respectively. White arrowheads in Snail1-HA xenografts: EMT-like phenotype.

differentiation (Batlle et al., 2002; de Lau et al., 2012; Holmberg et al., 2006; van der Flier et al., 2009; Verzi et al., 2011) and impaired self-renewal capacity of LS174T CRC cells. Anti-correlated expression of *SNAIL1* and for example the ISC factor *ASCL2* was also detected in the transcriptome data of colorectal carcinomas. It thus appears that SNAIL1-mediated activation of an EMT program can strongly compromise intestinal identity and stemness. Since ISCs or ISC-like cells are thought

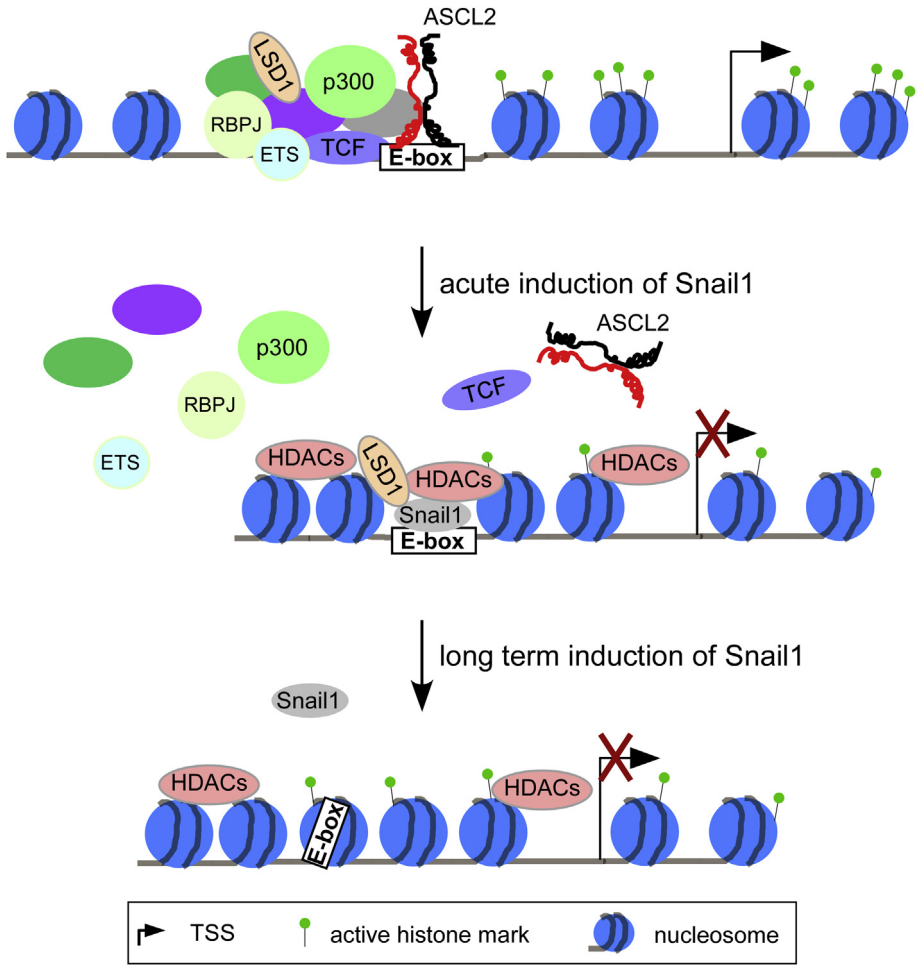

Figure 11 – Model for Snail1-mediated repression of *EPHB3*.

to be the cells of origin in CRC (Barker et al., 2009; Schwitalla et al., 2013) at first glance this appears difficult to reconcile with previous suggestions that EMT actually confers stemness in breast cancer (Mani et al., 2008; Morel et al., 2008) and more recent reports showing that SNAIL1 can promote cancer stem cell activities including symmetric cell division patterns also in colorectal cancer cells (Hwang et al., 2014, 2011). However, there are also other instances where EMT or the expression of EMT regulators interfere with stem cell features and the tumor initiation capacity of cells (Celia-Terrassa et al., 2012; Ocana et al., 2012; Tsai et al., 2012). Moreover, colorectal cancer is a heterogeneous disease which presents in a number of distinct subtypes (Cancer Genome Atlas, 2012; De Sousa et al., 2013; Loboda et al., 2011; Sadanandam et al., 2013). Thus, it is conceivable that in some cases CRC cancer stem cell capacity is reliant on SNAIL1 whereas in other instances stemness features can be maintained or acquired independently of SNAIL1 due to the origination of tumors from ISCs or ISC-like cells. A molecular explanation for the variable impact of SNAIL1 on stemness properties of CRC cells may be provided by differences in the genetic alterations that are characteristic for different CRC subtypes and that are represented in CRC cell lines (De Sousa et al., 2013; Sadanandam et al., 2013). For example, the SNAIL1-microRNA146a-Numb-β-catenin loop that was reported to control symmetric/asymmetric cell divisions, requires wild-type β-catenin (Hwang et al., 2014). Therefore, it is unlikely to be functional or implementable in LS174T and similar CRC cells which carry mutations in critical N-terminal phosporylation sites of β-catenin (Rowan et al., 2000). Clearly, the relationship between EMT and stemness is rather complex and may be influenced for example by tumor subtype-specific disturbances in signaling molecules and rewiring of regulatory networks in colorectal cancer (De Sousa et al., 2013; Sadanandam et al., 2013) and by pre-existing EMT features of organ-specific tissue resident stem cells as observed in the mammary gland (Guo et al., 2012).

EPHB receptors affect E-Cadherin adhesive properties and shedding (Cortina et al., 2007; Solanas et al., 2011). Prompted by the exceedingly rapid downregulation of *EPHB3* we investigated the significance of *EPHB3* inactivation for the initiation of EMT and showed that continued expression of *EPHB3* significantly opposes SNAIL1-induced EMT features *in vitro*. The results of our mouse xenograft model are in agreement with the *in vitro* observations and underscore the potent capacity of Snail1 to reorganize tumor and stromal architecture *in vivo* with concomitant downregulation of EPHB3 and E-Cadherin in corresponding tumor cell clusters. Importantly, phenotypic changes of CRC cells induced by Snail1-HA are attenuated by

sustained EPHB3 expression also *in vivo*. Overall, these findings underpin the importance of EPHB3 as tumor/invasion suppressor and raises the possibility that early loss of EPHB3 promotes the destabilization of epithelial cell features by targeting E-Cadherin protein function well before the manifestation of *CDH1* transcriptional repression. Further analyses have to reveal whether inactivation of the E-Cadherin protein and downregulation of its gene are indeed facilitated once *EPHB3* expression is lost and how EPHB3 mediates its protective effect on the molecular level. Together, our data clearly identify *EPHB3* as a novel target of SNAIL1 and suggest that disabling EPHB3 signaling is an important aspect to eliminate a roadblock at the onset of EMT processes in colorectal cancer.

Acknowledgments

We are grateful to T. Brabletz, E. Batlle, T. Brummer, C. Dive, O. Schilling, T. Reinheckel, M. Stemmler, A. García de Herreros and H. Munshi for gift of plasmids and cell lines; K. Geiger, J. Block and N. Bittermann for excellent technical assistance. This work was supported by grants from the Deutsche Forschungsgemeinschaft (DFG CRC-850 subprojects B3 to R.S., B5 to A. H., Z1 to S. L. and Z2 to R. Z.; CRC-992 subproject B01 to R.S.; CRC-746 subproject P2 to R.S.; Schu 688/9-1 and Schu688/12-1 to R.S.). K. Rönsch was supported by a fellowship from the Studienstiftung des deutschen Volkes.

Appendix A. Supplementary data

Supplementary data related to this article can be found at http://dx.doi.org/10.1016/j.molonc.2014.08.016.

REFERENCES

Ahmed, D., Eide, P.W., Eilertsen, I.A., Danielsen, S.A., Eknaes, M., Hektoen, M., Lind, G.E., Lothe, R.A., 2013. Epigenetic and genetic features of 24 colon cancer cell lines. Oncogenesis 2, e71.

Alter, O., Brown, P.O., Botstein, D., 2000. Singular value decomposition for genome-wide expression data processing and modeling. Proc. Natl. Acad. Sci. U.S.A. 97, 10101–10106.

American Cancer Society, 2013. Cancer Facts & Figures 2013. American Cancer Society, Atlanta, Ga.

Barker, N., Ridgway, R.A., van Es, J.H., van de Wetering, M., Begthel, H., van den Born, M., Danenberg, E., Clarke, A.R., Sansom, O.J., Clevers, H., 2009. Crypt stem cells as the cells-of-origin of intestinal cancer. Nature 457, 608–611.

Batlle, E., Bacani, J., Begthel, H., Jonkheer, S., Gregorieff, A., van de Born, M., Malats, N., Sancho, E., Boon, E., Pawson, T., Gallinger, S., Pals, S., Clevers, H., 2005. EphB receptor activity suppresses colorectal cancer progression. Nature 435, 1126–1130.

Batlle, E., Henderson, J.T., Beghtel, H., van den Born, M.M., Sancho, E., Huls, G., Meeldijk, J., Robertson, J., van de Wetering, M., Pawson, T., Clevers, H., 2002. Beta-catenin and TCF mediate cell positioning in the intestinal epithelium by controlling the expression of EphB/ephrinB. Cell 111, 251–263.

Calo, E., Wysocka, J., 2013. Modification of enhancer chromatin: what, how, and why? Mol. Cell 49, 825–837.

Cancer Genome Atlas, N, 2012. Comprehensive molecular characterization of human colon and rectal cancer. Nature 487, 330–337.

Celia-Terrassa, T., Meca-Cortes, O., Mateo, F., de Paz, A.M., Rubio, N., Arnal-Estape, A., Ell, B.J., Bermudo, R., Diaz, A., Guerra-Rebollo, M., Lozano, J.J., Estaras, C., Ulloa, C., Alvarez-Simon, D., Mila, J., Vilella, R., Paciucci, R., Martinez-Balbas, M., de Herreros, A.G., Gomis, R.R., Kang, Y., Blanco, J., Fernandez, P.L., Thomson, T.M., 2012. Epithelial-mesenchymal transition can suppress major attributes of human epithelial tumor-initiating cells. J. Clin. Inv. 122, 1849–1868.

Chiu, S.T., Chang, K.J., Ting, C.H., Shen, H.C., Li, H., Hsieh, F.J., 2009. Over-expression of EphB3 enhances cell-cell contacts and suppresses tumor growth in HT-29 human colon cancer cells. Carcinogenesis 30, 1475–1486.

Cortina, C., Palomo-Ponce, S., Iglesias, M., Fernandez-Masip, J.L., Vivancos, A., Whissell, G., Huma, M., Peiro, N., Gallego, L., Jonkheer, S., Davy, A., Lloreta, J., Sancho, E., Batlle, E., 2007. EphB-ephrin-B interactions suppress colorectal cancer progression by compartmentalizing tumor cells. Nat. Gen. 39, 1376–1383.

Dalerba, P., Kalisky, T., Sahoo, D., Rajendran, P.S., Rothenberg, M.E., Leyrat, A.A., Sim, S., Okamoto, J., Johnston, D.M., Qian, D., Zabala, M., Bueno, J., Neff, N.F., Wang, J., Shelton, A.A., Visser, B., Hisamori, S., Shimono, Y., van de Wetering, M., Clevers, H., Clarke, M.F., Quake, S.R., 2011. Single-cell dissection of transcriptional heterogeneity in human colon tumors. Nat. Biotech. 29, 1120–1127.

de Lau, W.B., Snel, B., Clevers, H.C., 2012. The R-spondin protein family. Genome Biol. 13, 242.

De Sousa, E.M.F., Wang, X., Jansen, M., Fessler, E., Trinh, A., de Rooij, L.P., de Jong, J.H., de Boer, O.J., van Leersum, R., Bijlsma, M.F., Rodermond, H., van der Heijden, M., van Noesel, C.J., Tuynman, J.B., Dekker, E., Markowetz, F., Medema, J.P., Vermeulen, L., 2013. Poor-prognosis colon cancer is defined by a molecularly distinct subtype and develops from serrated precursor lesions. Nat. Med. 19, 614–618.

Edlund, K., Larsson, O., Ameur, A., Bunikis, I., Gyllensten, U., Leroy, B., Sundstrom, M., Micke, P., Botling, J., Soussi, T., 2012. Data-driven unbiased curation of the TP53 tumor suppressor gene mutation database and validation by ultradeep sequencing of human tumors. Proc. Natl. Acad. Sci. U.S.A. 109, 9551–9556.

Fre, S., Pallavi, S.K., Huyghe, M., Lae, M., Janssen, K.P., Robine, S., Artavanis-Tsakonas, S., Louvard, D., 2009. Notch and Wnt signals cooperatively control cell proliferation and tumorigenesis in the intestine. Proc. Natl. Acad. Sci. U.S.A. 106, 6309–6314.

Furusawa, T., Moribe, H., Kondoh, H., Higashi, Y., 1999. Identification of CtBP1 and CtBP2 as corepressors of zinc finger-homeodomain factor deltaEF1. Mol. Cell. Biol. 19, 8581–8590.

Giresi, P.G., Kim, J., McDaniell, R.M., Iyer, V.R., Lieb, J.D., 2007. FAIRE (Formaldehyde-Assisted Isolation of Regulatory Elements) isolates active regulatory elements from human chromatin. Genome Res. 17, 877–885.

Guo, W., Keckesova, Z., Donaher, J.L., Shibue, T., Tischler, V., Reinhardt, F., Itzkovitz, S., Noske, A., Zurrer-Hardi, U., Bell, G., Tam, W.L., Mani, S.A., van Oudenaarden, A., Weinberg, R.A., 2012. Slug and Sox9 cooperatively determine the mammary stem cell state. Cell 148, 1015–1028.

Hatzis, P., van der Flier, L.G., van Driel, M.A., Guryev, V., Nielsen, F., Denissov, S., Nijman, I.J., Koster, J., Santo, E.E., Welboren, W., Versteeg, R., Cuppen, E., van de Wetering, M., Clevers, H., Stunnenberg, H.G., 2008. Genome-wide pattern of

TCF7L2/TCF4 chromatin occupancy in colorectal cancer cells. Mol. Cell. Biol. 28, 2732–2744.
Hirsch, C., Campano, L.M., Wohrle, S., Hecht, A., 2007. Canonical Wnt signaling transiently stimulates proliferation and enhances neurogenesis in neonatal neural progenitor cultures. Exp. Cell Res. 313, 572–587.
Holmberg, J., Genander, M., Halford, M.M., Anneren, C., Sondell, M., Chumley, M.J., Silvany, R.E., Henkemeyer, M., Frisen, J., 2006. EphB receptors coordinate migration and proliferation in the intestinal stem cell niche. Cell 125, 1151–1163.
Hu, Y., Smyth, G.K., 2009. ELDA: extreme limiting dilution analysis for comparing depleted and enriched populations in stem cell and other assays. J. Immunol. Meth. 347, 70–78.
Hwang, W.L., Jiang, J.K., Yang, S.H., Huang, T.S., Lan, H.Y., Teng, H.W., Yang, C.Y., Tsai, Y.P., Lin, C.H., Wang, H.W., Yang, M.H., 2014. MicroRNA-146a directs the symmetric division of Snail-dominant colorectal cancer stem cells. Nat. Cell Biol. 16, 268–280.
Hwang, W.L., Yang, M.H., Tsai, M.L., Lan, H.Y., Su, S.H., Chang, S.C., Teng, H.W., Yang, S.H., Lan, Y.T., Chiou, S.H., Wang, H.W., 2011. SNAIL regulates interleukin-8 expression, stem cell-like activity, and tumorigenicity of human colorectal carcinoma cells. Gastroenterology 141, 279–291, 291 e271–275.
Itzkovitz, S., Lyubimova, A., Blat, I.C., Maynard, M., van Es, J., Lees, J., Jacks, T., Clevers, H., van Oudenaarden, A., 2012. Single-molecule transcript counting of stem-cell markers in the mouse intestine. Nat. Cell Biol. 14, 106–114.
Jägle, S., Rönsch, K., Timme, S., Andrlová, H., Bertrand, M., Jäger, M., Proske, A., Schrempp, M., Yousaf, A., Michoel, T., Zeiser, R., Werner, M., Lassmann, S., Hecht, A., 2014. Silencing of the EPHB3 tumor-suppressor gene in human colorectal cancer through decommissioning of a transcriptional enhancer. Proc. Natl. Acad. Sci. U.S.A. 111, 4886–4891.
Kalluri, R., Weinberg, R.A., 2009. The basics of epithelial-mesenchymal transition. J. Clin. Inv. 119, 1420–1428.
Langfelder, P., Horvath, S., 2007. Eigengene networks for studying the relationships between co-expression modules. BMC Syst. Biol. 1, 54.
Liang, C.C., Park, A.Y., Guan, J.L., 2007. In vitro scratch assay: a convenient and inexpensive method for analysis of cell migration in vitro. Nat. Protoc. 2, 329–333.
Lin, T., Ponn, A., Hu, X., Law, B.K., Lu, J., 2010a. Requirement of the histone demethylase LSD1 in Snai1-mediated transcriptional repression during epithelial-mesenchymal transition. Oncogene 29, 4896–4904.
Lin, Y., Wu, Y., Li, J., Dong, C., Ye, X., Chi, Y.I., Evers, B.M., Zhou, B.P., 2010b. The SNAG domain of Snail1 functions as a molecular hook for recruiting lysine-specific demethylase 1. EMBO J. 29, 1803–1816.
Loboda, A., Nebozhyn, M.V., Watters, J.W., Buser, C.A., Shaw, P.M., Huang, P.S., Van't Veer, L., Tollenaar, R.A., Jackson, D.B., Agrawal, D., Dai, H., Yeatman, T.J., 2011. EMT is the dominant program in human colon cancer. BMC Med. Genomics 4, 9.
Mani, S.A., Guo, W., Liao, M.J., Eaton, E.N., Ayyanan, A., Zhou, A.Y., Brooks, M., Reinhard, F., Zhang, C.C., Shipitsin, M., Campbell, L.L., Polyak, K., Brisken, C., Yang, J., Weinberg, R.A., 2008. The epithelial-mesenchymal transition generates cells with properties of stem cells. Cell 133, 704–715.
Marisa, L., de Reynies, A., Duval, A., Selves, J., Gaub, M.P., Vescovo, L., Etienne-Grimaldi, M.C., Schiappa, R., Guenot, D., Ayadi, M., Kirzin, S., Chazal, M., Flejou, J.F., Benchimol, D., Berger, A., Lagarde, A., Pencreach, E., Piard, F., Elias, D., Parc, Y., Olschwang, S., Milano, G., Laurent-Puig, P., Boige, V., 2013. Gene expression classification of colon cancer into molecular subtypes: characterization, validation, and prognostic value. PLoS Med. 10, e1001453.
Metzger, E., Wissmann, M., Yin, N., Muller, J.M., Schneider, R., Peters, A.H., Gunther, T., Buettner, R., Schule, R., 2005. LSD1 demethylates repressive histone marks to promote androgen-receptor-dependent transcription. Nature 437, 436–439.
Morel, A.P., Lievre, M., Thomas, C., Hinkal, G., Ansieau, S., Puisieux, A., 2008. Generation of breast cancer stem cells through epithelial-mesenchymal transition. PLoS One 3, e2888.
Mouradov, D., Sloggett, C., Jorissen, R.N., Love, C.G., Li, S., Burgess, A.W., Arango, D., Strausberg, R.L., Buchanan, D., Wormald, S., O'Connor, L., Wilding, J.L., Bicknell, D., Tomlinson, I.P., Bodmer, W.F., Mariadason, J.M., Sieber, O.M., 2014. Colorectal cancer cell lines are representative models of the main molecular subtypes of primary cancer. Cancer Res. 74, 3238–3247.
Munoz, J., Stange, D.E., Schepers, A.G., van de Wetering, M., Koo, B.K., Itzkovitz, S., Volckmann, R., Kung, K.S., Koster, J., Radulescu, S., Myant, K., Versteeg, R., Sansom, O.J., van Es, J.H., Barker, N., van Oudenaarden, A., Mohammed, S., Heck, A.J., Clevers, H., 2012. The Lgr5 intestinal stem cell signature: robust expression of proposed quiescent '+4' cell markers. EMBO J. 31, 3079–3091.
O'Brien, C.A., Kreso, A., Ryan, P., Hermans, K.G., Gibson, L., Wang, Y., Tsatsanis, A., Gallinger, S., Dick, J.E., 2012. ID1 and ID3 regulate the self-renewal capacity of human colon cancer-initiating cells through p21. Cancer Cell 21, 777–792.
Ocana, O.H., Corcoles, R., Fabra, A., Moreno-Bueno, G., Acloque, H., Vega, S., Barrallo-Gimeno, A., Cano, A., Nieto, M.A., 2012. Metastatic colonization requires the repression of the epithelial-mesenchymal transition inducer Prrx1. Cancer Cell 22, 709–724.
Peinado, H., Ballestar, E., Esteller, M., Cano, A., 2004. Snail mediates E-cadherin repression by the recruitment of the Sin3A/histone deacetylase 1 (HDAC1)/HDAC2 complex. Mol. Cell. Biol 24, 306–319.
Peinado, H., Olmeda, D., Cano, A., 2007. Snail, Zeb and bHLH factors in tumour progression: an alliance against the epithelial phenotype? Nat. Rev. Cancer 7, 415–428.
Pena, C., Garcia, J.M., Silva, J., Garcia, V., Rodriguez, R., Alonso, I., Millan, I., Salas, C., de Herreros, A.G., Munoz, A., Bonilla, F., 2005. E-cadherin and vitamin D receptor regulation by SNAIL and ZEB1 in colon cancer: clinicopathological correlations. Hum. Mol. Gen. 14, 3361–3370.
Rodilla, V., Villanueva, A., Obrador-Hevia, A., Robert-Moreno, A., Fernandez-Majada, V., Grilli, A., Lopez-Bigas, N., Bellora, N., Alba, M.M., Torres, F., Dunach, M., Sanjuan, X., Gonzalez, S., Gridley, T., Capella, G., Bigas, A., Espinosa, L., 2009. Jagged1 is the pathological link between Wnt and Notch pathways in colorectal cancer. Proc. Natl. Acad. Sci. U.S.A. 106, 6315–6320.
Rönsch, K., Jäger, M., Schopflin, A., Danciu, M., Lassmann, S., Hecht, A., 2011. Class I and III HDACs and loss of active chromatin features contribute to epigenetic silencing of CDX1 and EPHB tumor suppressor genes in colorectal cancer. Epigenetics 6, 610–622.
Rowan, A.J., Lamlum, H., Ilyas, M., Wheeler, J., Straub, J., Papadopoulou, A., Bicknell, D., Bodmer, W.F., Tomlinson, I.P., 2000. APC mutations in sporadic colorectal tumors: a mutational "hotspot" and interdependence of the "two hits". Proc. Natl. Acad. Sci. U.S.A. 97, 3352–3357.
Sadanandam, A., Lyssiotis, C.A., Homicsko, K., Collisson, E.A., Gibb, W.J., Wullschleger, S., Ostos, L.C., Lannon, W.A., Grotzinger, C., Del Rio, M., Lhermitte, B., Olshen, A.B., Wiedenmann, B., Cantley, L.C., Gray, J.W., Hanahan, D., 2013. A colorectal cancer classification system that associates cellular phenotype and responses to therapy. Nat. Med. 19, 619–625.
Schwitalla, S., Fingerle, A.A., Cammareri, P., Nebelsiek, T., Goktuna, S.I., Ziegler, P.K., Canli, O., Heijmans, J., Huels, D.J.,

Moreaux, G., Rupec, R.A., Gerhard, M., Schmid, R., Barker, N., Clevers, H., Lang, R., Neumann, J., Kirchner, T., Taketo, M.M., van den Brink, G.R., Sansom, O.J., Arkan, M.C., Greten, F.R., 2013. Intestinal tumorigenesis initiated by dedifferentiation and acquisition of stem-cell-like properties. Cell 152, 25–38.

Shioiri, M., Shida, T., Koda, K., Oda, K., Seike, K., Nishimura, M., Takano, S., Miyazaki, M., 2006. Slug expression is an independent prognostic parameter for poor survival in colorectal carcinoma patients. Br. J. Cancer 94, 1816–1822.

Solanas, G., Cortina, C., Sevillano, M., Batlle, E., 2011. Cleavage of E-cadherin by ADAM10 mediates epithelial cell sorting downstream of EphB signalling. Nat. Cell Biol. 13, 1100–1107.

Soleimani, V.D., Yin, H., Jahani-Asl, A., Ming, H., Kockx, C.E., van Ijcken, W.F., Grosveld, F., Rudnicki, M.A., 2012. Snail regulates MyoD binding-site occupancy to direct enhancer switching and differentiation-specific transcription in myogenesis. Mol. Cell 47, 457–468.

Stringer, E.J., Duluc, I., Saandi, T., Davidson, I., Bialecka, M., Sato, T., Barker, N., Clevers, H., Pritchard, C.A., Winton, D.J., Wright, N.A., Freund, J.N., Deschamps, J., Beck, F., 2012. Cdx2 determines the fate of postnatal intestinal endoderm. Development 139, 465–474.

Tsai, J.H., Donaher, J.L., Murphy, D.A., Chau, S., Yang, J., 2012. Spatiotemporal regulation of epithelial-mesenchymal transition is essential for squamous cell carcinoma metastasis. Cancer Cell 22, 725–736.

Valastyan, S., Weinberg, R.A., 2011. Tumor metastasis: molecular insights and evolving paradigms. Cell 147, 275–292.

van de Wetering, M., Sancho, E., Verweij, C., de Lau, W., Oving, I., Hurlstone, A., van der Horn, K., Batlle, E., Coudreuse, D., Haramis, A.P., Tjon-Pon-Fong, M., Moerer, P., van den Born, M., Soete, G., Pals, S., Eilers, M., Medema, R., Clevers, H., 2002. The beta-catenin/TCF-4 complex imposes a crypt progenitor phenotype on colorectal cancer cells. Cell 111, 241–250.

van der Flier, L.G., Clevers, H., 2009. Stem cells, self-renewal, and differentiation in the intestinal epithelium. Ann. Rev. Phys. 71, 241–260.

van der Flier, L.G., van Gijn, M.E., Hatzis, P., Kujala, P., Haegebarth, A., Stange, D.E., Begthel, H., van den Born, M., Guryev, V., Oving, I., van Es, J.H., Barker, N., Peters, P.J., van de Wetering, M., Clevers, H., 2009. Transcription factor achaete scute-like 2 controls intestinal stem cell fate. Cell 136, 903–912.

van Es, J.H., van Gijn, M.E., Riccio, O., van den Born, M., Vooijs, M., Begthel, H., Cozijnsen, M., Robine, S., Winton, D.J., Radtke, F., Clevers, H., 2005. Notch/gamma-secretase inhibition turns proliferative cells in intestinal crypts and adenomas into goblet cells. Nature 435, 959–963.

Veeman, M.T., Slusarski, D.C., Kaykas, A., Louie, S.H., Moon, R.T., 2003. Zebrafish prickle, a modulator of noncanonical Wnt/Fz signaling, regulates gastrulation movements. Curr. Biol. 13, 680–685.

Verzi, M.P., Shin, H., Ho, L.L., Liu, X.S., Shivdasani, R.A., 2011. Essential and redundant functions of caudal family proteins in activating adult intestinal genes. Mol. Cell. Biol. 31, 2026–2039.

von Burstin, J., Eser, S., Paul, M.C., Seidler, B., Brandl, M., Messer, M., von Werder, A., Schmidt, A., Mages, J., Pagel, P., Schnieke, A., Schmid, R.M., Schneider, G., Saur, D., 2009. E-cadherin regulates metastasis of pancreatic cancer in vivo and is suppressed by a SNAIL/HDAC1/HDAC2 repressor complex. Gastroenterology 137, 361–371, 371 e361–365.

Wallmen, B., Schrempp, M., Hecht, A., 2012. Intrinsic properties of Tcf1 and Tcf4 splice variants determine cell-type-specific Wnt/beta-catenin target gene expression. Nucl. Acids Res. 40, 9455–9469.

Wang, Y., Ngo, V.N., Marani, M., Yang, Y., Wright, G., Staudt, L.M., Downward, J., 2010. Critical role for transcriptional repressor Snail2 in transformation by oncogenic RAS in colorectal carcinoma cells. Oncogene 29, 4658–4670.

Weise, A., Bruser, K., Elfert, S., Wallmen, B., Wittel, Y., Wohrle, S., Hecht, A., 2010. Alternative splicing of Tcf7l2 transcripts generates protein variants with differential promoter-binding and transcriptional activation properties at Wnt/beta-catenin targets. Nucl. Acids Res. 38, 1964–1981.

Welman, A., Barraclough, J., Dive, C., 2006. Generation of cells expressing improved doxycycline-regulated reverse transcriptional transactivator rtTA2S-M2. Nat. Protoc. 1, 803–811.

Woodford-Richens, K.L., Rowan, A.J., Gorman, P., Halford, S., Bicknell, D.C., Wasan, H.S., Roylance, R.R., Bodmer, W.F., Tomlinson, I.P., 2001. SMAD4 mutations in colorectal cancer probably occur before chromosomal instability, but after divergence of the microsatellite instability pathway. Proc. Natl. Acad. Sci. U.S.A. 98, 9719–9723.

Yatim, A., Benne, C., Sobhian, B., Laurent-Chabalier, S., Deas, O., Judde, J.G., Lelievre, J.D., Levy, Y., Benkirane, M., 2012. NOTCH1 nuclear interactome reveals key regulators of its transcriptional activity and oncogenic function. Mol. Cell 48, 445–458.